

Modelling the Role of Angiogenesis and Vasculogenesis in Solid Tumour Growth

I.J. Stamper^{a,*}, H.M. Byrne^a, M.R. Owen^a, P.K. Maini^{b,c}

^aCentre for Mathematical Medicine, School of Mathematical Sciences, University of Nottingham, Nottingham NG7 2RD, UK

^bCentre for Mathematical Biology, Mathematical Institute, University of Oxford, 24-29 St Giles', Oxford OX1 3LB, UK

^cOxford Centre for Integrative Systems Biology, Dept. of Biochemistry, South Parks Road, Oxford OX1 3QU, UK

Received: 13 September 2006 / Accepted: 14 June 2007 / Published online: 15 September 2007
© Society for Mathematical Biology 2007

Abstract Recent experimental evidence suggests that vasculogenesis may play an important role in tumour vascularisation. While angiogenesis involves the proliferation and migration of endothelial cells (ECs) in pre-existing vessels, vasculogenesis involves the mobilisation of bone-marrow-derived endothelial progenitor cells (EPCs) into the bloodstream. Once blood-borne, EPCs home in on the tumour site, where subsequently they may differentiate into ECs and form vascular structures.

In this paper, we develop a mathematical model, formulated as a system of nonlinear ordinary differential equations (ODEs), which describes vascular tumour growth with both angiogenesis and vasculogenesis contributing to vessel formation. Submodels describing exclusively angiogenic and exclusively vasculogenic tumours are shown to exhibit similar growth dynamics. In each case, there are three possible scenarios: the tumour remains in an avascular steady state, the tumour evolves to a vascular equilibrium, or unbounded vascular growth occurs. Analysis of the full model reveals that these three behaviours persist when angiogenesis and vasculogenesis act simultaneously. However, when both vascularisation mechanisms are active, the tumour growth rate may increase, causing the tumour to evolve to a larger equilibrium size or to expand uncontrollably. Alternatively, the growth rate may be left unaffected, which occurs if either vascularisation process alone is able to keep pace with the demands of the growing tumour.

To clarify further the effects of vasculogenesis, the full model is also used to compare possible treatment strategies, including chemotherapy and antiangiogenic therapies aimed at suppressing vascularisation. This investigation highlights how, dependent on model parameter values, targeting both ECs and EPCs may be necessary in order to effectively reduce tumour vasculature and inhibit tumour growth.

Keywords Tumour growth · Angiogenesis · Vasculogenesis · Endothelial progenitor cell · Therapy

*Corresponding author.

E-mail address: pmxijs@nottingham.ac.uk (I.J. Stamper).

1. Introduction

The association between angiogenesis and solid tumour growth has been investigated extensively since the early 1970s (Folkman, 1971). Angiogenesis is characterised by sprouting from pre-existing vessels via the migration and proliferation of endothelial cells (ECs) and it is now well known that tumours, often as a result of hypoxia, secrete tumour angiogenic factors (TAFs) which stimulate angiogenesis (Mantzaris et al., 2004). More recently, vasculogenesis has been shown to contribute to the vasculature in solid tumours (Boltontrade et al., 2002; Duda et al., 2006; Li et al., 2004; Lyden et al., 2001; Peters et al., 2005; Spring et al., 2005). Originally vasculogenesis, or blood vessel formation *de novo*, was thought to occur only during embryogenesis when stem cells (angioblasts) differentiate from mesoderm, and aggregate, align and differentiate into ECs to form the first vascular networks (Drake, 2003; Risau and Flamme, 1995). Postnatal vasculogenesis was not reported until 1997, when endothelial progenitor cells (EPCs), found in the blood of adult individuals, were shown to induce postnatal vasculogenesis at ischemic sites (Asahara et al., 1997). During postnatal vasculogenesis, EPCs are recruited from the bone marrow into the blood and incorporate into vascular structures at the site of neovascularisation by proliferating and differentiating into ECs (see Fig. 1) (Hristov et al., 2003; Hunting et al., 2005; Khakoo and Finkel, 2005; Rafii et al., 2002; Ribatti, 2004; Tepper et al., 2005; Vajkoczy et al., 2003). One substance known to mobilise EPCs from the bone marrow is vascular endothelial growth factor (VEGF) (Asahara et al., 1999; Hattori et al., 2001). VEGF is closely correlated with tumour neovascularisation and is secreted by tumour cells, for example during hypoxia (Harris, 2002). Since increased levels of VEGF have been observed in the blood of patients with certain cancers (Hoeben et al., 2004; Kolomecki et al., 2001), it is possible that tumour-induced mobilisation of EPCs could occur. At present, there is no consensus on whether the level of EPCs in the blood of cancer patients is elevated (Dome et al., 2006; Kim et al., 2003; Sussman et al., 2003).

The relative importance of vasculogenesis in postnatal conditions, for example tumour vascularisation, is also still heavily disputed. The fraction of vessels formed by vasculogenesis in experimental tumour models ranges from very high to nonexistent (Aghi and Chiocca, 2005). These discrepancies could be related to differences in the tumour strain, the tumour site or microenvironment or to the implementation and the time scale of the experiments (Aghi and Chiocca, 2005). The discrepancies might also be attributed to the difficulties in defining EPCs and distinguishing them from circulating ECs and from other circulating bone-marrow-derived cells (Hunting et al., 2005; Khakoo and Finkel, 2005). The data from human tumours are scarce. In one study of six human tumour samples (obtained from patients who had received bone marrow transplants from donors of the opposite sex and later developed cancer), the contribution of EPCs varied from 1% to 12% (Peters et al., 2005).

Previously, only two mathematical models have been developed to investigate the importance of vasculogenesis in solid tumour growth (Komarova and Mironov, 2005; Stoll et al., 2003). In Stoll et al. (2003), tumour growth is assumed to depend on the total vascular density, i.e. both angiogenesis- and vasculogenesis-derived vessels. The vasculogenic contribution is determined by using a compartmental model of ordinary differential equations (ODEs) that predicts the level of EPCs and TAF in the blood and the bone marrow. The ODE model is then coupled with partial differential equations (PDEs) that

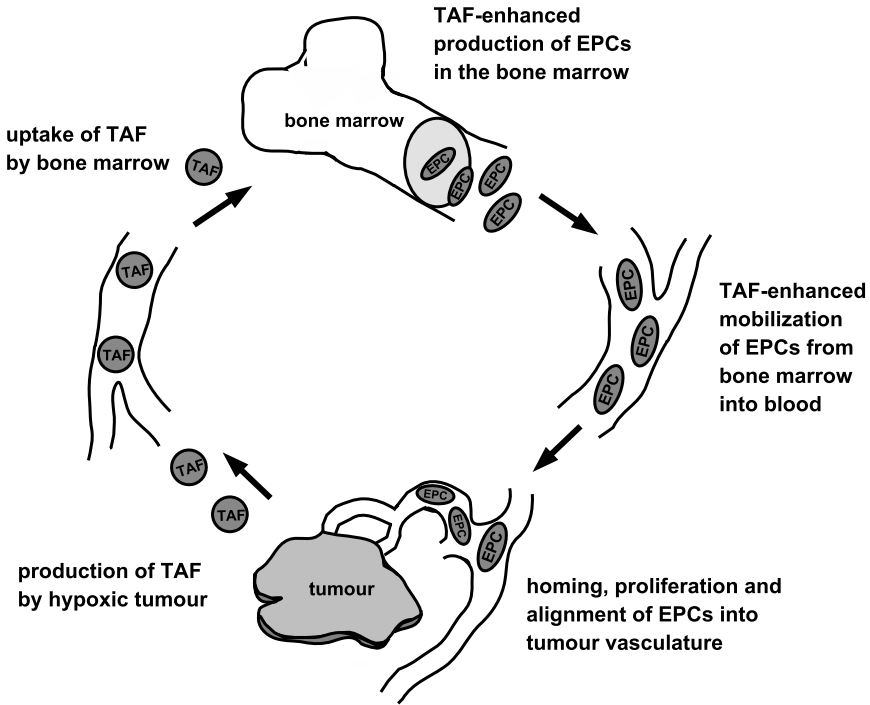


Fig. 1 Illustration of tumour-induced vasculogenesis. EPCs are produced in the bone marrow. The tumour's secretion of angiogenic factors, which diffuse into the blood, may increase the production of EPCs in the bone marrow and mobilise EPCs into the bloodstream. EPCs travel through the bloodstream and home in on the tumour vasculature, possibly influenced by high levels of angiogenic factors at the tumour site. Subsequently, the EPCs progress into the tumour interstitium where they start to form clusters and align themselves into new vessels.

describe a radially-symmetric, expanding tumour mass. Using their model (Stoll et al., 2003), Stoll et al. were able to predict that EPCs can contribute appreciably to both the vascular density and the tumour growth rate. They also showed that combination treatments which target both local and systemic parts of the vascularisation process are the most effective at inhibiting tumour growth. In common with Stoll et al., Komarova and Mironov (2005) also distinguish between three compartments (the bone marrow, the blood and the tumour). However, their model is simpler, being fully spatially-averaged and neglecting the concentrations of TAF. The predictions in Komarova and Mironov (2005) are that for tumours which only acquire new vasculature by angiogenesis, the tumour mass grows as a cubic power of time. If, however, only vasculogenesis is responsible for the neovasculature, tumours will grow faster than linearly initially, and linearly at large times. Furthermore, Komarova and Mironov predict that vasculogenesis will result in a decline in the level of EPCs in the bone marrow. In the blood, the number of EPCs will tend to zero at large times, possibly after having gone up initially.

The model we derive in this paper describes the development of a small solid tumour from an avascular state to an early stage of vascularisation. In order to keep the model as

simple as possible and amenable to analysis, we construct a compartmental ODE model, as was done in Komarova and Mironov (2005). However, while focusing on a minimal model, we still include some new features that were not considered in Komarova and Mironov (2005) and Stoll et al. (2003). For example, we include TAF explicitly, indirectly linking its production to hypoxia by assuming that its rate of production increases as the vascular density (and hence, the concentration of oxygen) decreases. While Stoll et al. included TAF explicitly, there the net angiogenic activity did not appear to be related to the microenvironment, e.g. hypoxia. Another new phenomenon that we incorporate is the occlusion of newly formed vessels. Occlusion is believed to occur as a result of the increase in mechanical pressure exerted on the immature vessels by rapidly proliferating tumour cells (Griffon-Etienne et al., 1999; Helmlinger et al., 1997; Padera et al., 2004). As a result, we identify conditions under which the vascularised tumour evolves to a steady state. This contrasts with the behaviour in Komarova and Mironov (2005) where vascularisation always leads to unconstrained tumour growth.

The remainder of this paper is organised as follows. We derive our model in Section 2 and devote Section 3 to analysis of two submodels, one where angiogenesis dominates vessel formation and one where vasculogenesis is dominant. In addition to allowing extraction of generic features of angiogenic and vasculogenic tumour growth, this approach will enable comparisons with corresponding submodels in Komarova and Mironov (2005). In Section 4, we study the full model, investigating how the combined effects of angiogenesis and vasculogenesis affect tumour growth. We also show how our model can be used to predict a tumour's response to chemotherapy and antiangiogenic therapies. Finally, in Section 5, we discuss our results and compare them to experimental data and predictions from existing mathematical models (Komarova and Mironov, 2005; Stoll et al., 2003).

2. Model development

In this section, we develop our model, which consists of a system of nonlinear time-dependent ODEs. The model has three compartments: the bone marrow, the blood and the tumour, each of which are assumed to have a spatially uniform structure. We assume that the tumour cells rely on a blood supply to survive and proliferate, and that the tumour vasculature can develop via angiogenesis and vasculogenesis. To describe vasculogenesis, we introduce the dependent variables, x , y and z to denote the level of EPCs in the bone marrow, the blood and the tumour, respectively. Functional vessels created by EPCs through vasculogenesis are denoted by u , whereas vessels that arise from angiogenesis are denoted by w . Both u and w contribute to the total tumour vasculature volume, v , and hence to the growth rate of the tumour volume, m . We also allow for occlusion of the newly formed vessels at a rate which increases with the ratio of tumour volume to vessel volume. Furthermore, we assume that both vasculogenesis and angiogenesis are dependent on angiogenic factors and derive mass balance equations for the concentrations of TAF in the tumour, C_1 , in the blood, C_2 , and in the bone marrow, C_3 . A schematic diagram showing how the dependent variables interact is presented in Fig. 2 while tables listing the model variables and parameters are contained in the Appendix.

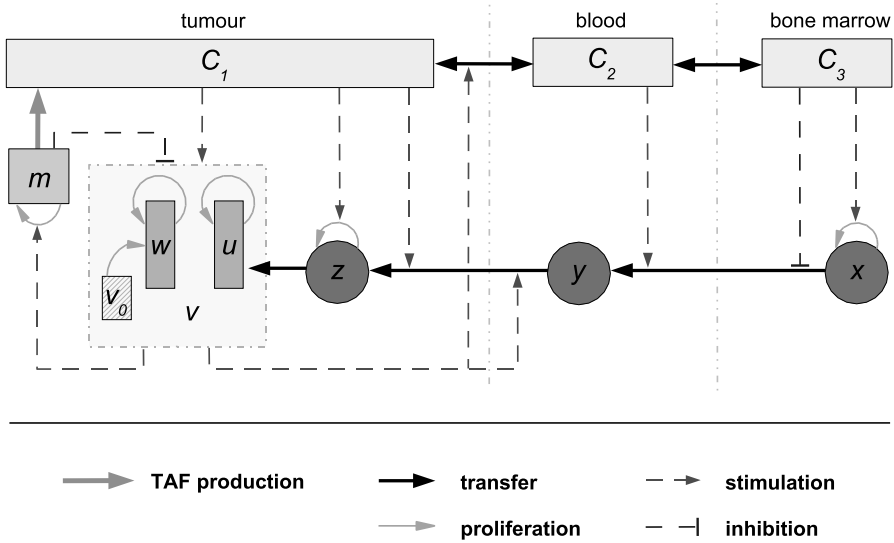


Fig. 2 Schematic diagram of our model showing how the dependent variables interact. The model has three compartments: the tumour, the blood and the bone marrow. The tumour production of TAF stimulates neovascularisation by angiogenesis and vasculogenesis, whereas the expanding tumour mass inhibits vessel formation through occlusion. An increase in tumour vasculature, in turn, enhances tumour growth. The model variables are: tumour volume, m ; concentration of TAF in the tumour, C_1 , in the blood, C_2 , and in the bone marrow, C_3 ; the level of EPCs in these compartments, x , y and z ; and total vasculature, v , which consists of angiogenic vessel volume, w , and vasculogenic vessel volume, u . The parameter v_0 represents the volume of pre-existing vasculature.

2.1. EPC dynamics

Since vasculogenesis involves EPCs (as illustrated in Fig. 1), we model their dynamics as they transit from the bone marrow to the blood and then to the tumour.

2.1.1. EPC levels in the bone marrow, $x(t)$

We assume that the level of EPCs in the bone marrow, $x(t)$, depends on their production and death (normal or due to apoptosis), as well as their delivery into the bloodstream. When no TAF is present, EPC production is assumed to occur at a constant rate, p_1 , whereas apoptosis and delivery to the blood occur at rates d_1x and k_1x , respectively. In Asahara et al. (1999) and Moore et al. (2001), chemotaxis (in response to VEGF) is suggested to cause enhanced EPC mobilisation into the circulation; we describe this effect by including a term of the form $k_2(C_2 - C_3)x$. This term models EPCs moving by chemotaxis toward regions of higher TAF concentration, across the wall of the blood vessels into the bloodstream. Another factor that may play a role in EPC mobilisation is matrix metalloprotease-9 (MMP-9). When MMP-9 is activated (e.g. in response to VEGF) it releases soluble Kit-ligand, which causes EPCs to move into the bone marrow vasculature (Heissig et al., 2002). Translocation into the vascular zone makes the EPCs more likely to enter the circulation, and transforms the cells from a quiescent to a proliferative state (Heissig et al., 2002). Accordingly, we assume that the production of EPCs increases in

the presence of TAF in the bone marrow and introduce an additional production term, p_2C_3 , to account for this. Combining the above factors, we arrive at the following equation:

$$\frac{dx}{dt} = \underbrace{p_1 + p_2C_3}_{\text{proliferation}} - \underbrace{k_1x - k_2(C_2 - C_3)x}_{\text{delivery into blood}} - \underbrace{d_1x}_{\text{apoptosis}}, \quad (1)$$

where p_1 , p_2 , k_1 , k_2 and d_1 are positive constants.

2.1.2. EPC levels in the blood, $y(t)$

For simplicity, we neglect EPC proliferation in the blood and assume that the level of EPCs in the bloodstream, $y(t)$, increases due to delivery from the bone marrow (see Eq. (1)) and decreases at a rate d_2y due to apoptosis and to EPC incorporation into other tissues. Circulating EPCs are, for instance, known to stick to vessel walls at active sites of neovascularisation, such as ischemic tissue (Tepper et al., 2005) and tumours (Vajkoczy et al., 2003). The factors that govern adherence to the vasculature are not completely understood. In Vajkoczy et al. (2003), the adhesion of EPCs was shown to be dependent on E- and P-selectin and glycoprotein ligand-1. Other factors that have been implicated in the homing of EPCs into the tumour vasculature are the integrin $\alpha_4\beta_1$ (Jin et al., 2006), as well as the local level of VEGF at the tumour site and the activation of its receptor VEGFR-1 (Li et al., 2006). In accordance with the notion that VEGF upregulates EPC adherence, we assume that it occurs at a rate k_3C_1vy . Thus we have:

$$\frac{dy}{dt} = \underbrace{k_1x + k_2(C_2 - C_3)x}_{\text{delivery from bone marrow}} - \underbrace{k_3C_1vy}_{\text{adherence to tumour}} - \underbrace{d_2y}_{\text{apoptosis/uptake by other organs}}, \quad (2)$$

where k_3 and d_2 are positive constants and v denotes the tumour vasculature.

2.1.3. EPC levels in the tumour, $z(t)$

In both ischemic tissue (Tepper et al., 2005) and tumours (Vajkoczy et al., 2003), EPC incorporation into vessels follows a similar pattern. After adhering to the vascular wall, the EPCs egress into the interstitium where they start to form cellular clusters and gradually align themselves into functional vessels. We therefore assume that the level of EPCs in the tumour, $z(t)$, increases at a rate k_3C_1vy due to EPC adherence to the tumour vasculature (see Eq. (2)). We also incorporate EPC proliferation, which was observed in Tepper et al. (2005) (when the EPC formed clusters) and is enhanced when TAF levels are high (Asahara et al., 1999), by assuming that it occurs at a rate p_3C_1z . We assume further that the level of EPCs in the tumour decreases at rate k_4z when EPCs align to form functional vessels and at rate d_3z due to apoptosis. Combining these ideas, we deduce that $z(t)$ satisfies:

$$\frac{dz}{dt} = \underbrace{k_3C_1vy}_{\text{adherence from blood}} + \underbrace{p_3C_1z}_{\text{proliferation}} - \underbrace{k_4z}_{\text{alignment into vessels}} - \underbrace{d_3z}_{\text{apoptosis}}, \quad (3)$$

where p_3 , k_4 and d_3 are positive constants.

2.2. *Tumour vasculature, $v(t)$*

The total tumour vasculature, $v(t)$, comprises the vasculogenic vasculature, $u(t)$, the angiogenic vasculature, $w(t)$, and a pre-existing constant background vasculature, v_0 , so that

$$v = w + u + v_0. \tag{4}$$

We include a constant background vasculature in (4) since the initiation of both angiogenesis and vasculogenesis requires vessels to be present in the vicinity of the tumour.

2.2.1. *Vessels created by angiogenesis, $w(t)$*

Even though angiogenesis is a complex process, the main mechanism involves the sprouting of new capillaries from pre-existing vessels and can be summarised by three phases (Mantzaris et al., 2004): activation of ECs by TAF (such as VEGF and basic fibroblast growth factor (bFGF)), migration and proliferation of ECs, and vessel maturation. During activation, the ECs respond to the tumour’s secretion of TAF, which, when bound to receptors on the surface of ECs, causes them to secrete enzymes, e.g. metalloproteinases (MMPs), that degrade the basement membrane and the extracellular matrix. Subsequently, new sprouts are able to form by EC migration toward the tumour, up spatial gradients of TAF, followed by EC proliferation. Finally, stabilisation of the vessels, through the acquisition of a pericyte and smooth muscle cell covering, concludes the angiogenic process. The stabilisation phase is usually incomplete in tumours, rendering the vessels leaky with a highly irregular flow (Carmeliet and Jain, 2000; Jain, 2003).

We assume that angiogenic vessel growth occurs at rate $p_4 C_1 (v_0 + w)$, i.e. it is proportional to the concentration of TAF in the tumour and to the volume of pre-existing and angiogenesis-derived vasculature. We also allow for vessel occlusion (Griffon-Etienne et al., 1999; Helmlinger et al., 1997; Padera et al., 2004), assuming that the rate of occlusion is low when the ratio of tumour volume to vasculature, m/v , is low, and that it increases to a maximum as m/v increases. This assumption is motivated by the increased pressure and compression that vessels experience as the average tumour mass per vessel increases. Assuming further that the vessels undergo apoptosis at a rate $d_4 w$ we obtain:

$$\frac{dw}{dt} = \underbrace{p_4 C_1 (v_0 + w)}_{\text{proliferation}} - \underbrace{\frac{\delta_1 m w}{m + \delta_2 v}}_{\text{occlusion}} - \underbrace{d_4 w}_{\text{apoptosis}}, \tag{5}$$

where p_4 , δ_1 , δ_2 and d_4 are positive constants. We observe here that if TAF is absent ($C_1 = 0$), then $\dot{w} < 0$ and the vessels will regress, i.e. our vessels correspond to newly-formed, immature vessels that depend on TAF (VEGF) for their survival (Carmeliet, 2003; Hoeben et al., 2004).

2.2.2. *Vessels created by vasculogenesis, $u(t)$*

The rate at which vasculogenic vessels are created from EPCs is proportional to the alignment term in (3) with a conversion factor, μ , which converts the number of EPCs that per unit time arrange themselves into functional vessels, into units of volume. Here we

point out that it is not known at what point during vasculogenesis EPCs differentiate into ECs (Schatteman and Awad, 2004). However, we assume that once the EPCs contribute to functional vessels they behave as ECs, i.e. the vasculogenic vessels may become occluded, undergo apoptosis and proliferate in response to angiogenic factors. This means that the net contribution from EPCs to the tumour vasculature stems from a purely vasculogenic part (involving mobilisation from the bone marrow, adherence to the tumour site and incorporation into vessels), and an angiogenic part (involving subsequent TAF-induced proliferation). We therefore obtain:

$$\frac{du}{dt} = \underbrace{\mu k_4 z}_{\text{EPC alignment into vessels}} + \underbrace{p_5 C_1 u}_{\text{proliferation}} - \underbrace{\frac{\delta_3 mu}{m + \delta_4 v}}_{\text{occlusion}} - \underbrace{d_5 u}_{\text{apoptosis}}, \tag{6}$$

where μ , p_5 , δ_3 , δ_4 and d_5 are positive constants. We remark that if the vasculogenic vessels have the same characteristics as angiogenesis-derived vessels, then $p_5 = p_4$, $\delta_3 = \delta_1$, $\delta_4 = \delta_2$ and $d_5 = d_4$.

2.3. Tumour volume, $m(t)$

We assume that the tumour volume, $m(t)$, which we consider to be a mix of tumour cells and interstitial material, grows at a rate proportional to both m and a saturable function of the ratio v/m . In particular, we assume that when v/m is large, the tumour cells experience optimal conditions for growth, receiving enough oxygen and nutrients from the vasculature to proliferate at their maximum rate. We also assume that the tumour cells undergo apoptosis at rate $d_0 m$ and by combining these effects we deduce that:

$$\frac{dm}{dt} = \underbrace{\frac{\beta vm}{v + \lambda m}}_{\text{proliferation}} - \underbrace{d_0 m}_{\text{apoptosis}}, \tag{7}$$

where β , λ and d_0 are positive constants. In describing the tumour volume in this way, we assume that tumour cells that die are degraded instantly, and thereafter do not contribute to the tumour volume.

2.4. Mass balance equations for TAF

The last step in our model derivation is to obtain mass balance equations for the concentrations of TAF in the tumour, the blood and the bone marrow. In a physiological pharmacokinetic model, each tissue is considered to consist of three phases: a vascular space, an interstitial space and a cellular space (Amidon et al., 2000; Gerlowski and Jain, 1983; Shargel and Yu, 1999). However, if the rate of mass transfer across the capillary wall and the cellular membrane is rapid compared to the tissue perfusion rate, the tissue can be assumed to be well mixed. Thus if the transfer is blood-flow-limited, then the TAF is homogeneously distributed within the vascular, interstitial and cellular spaces, and the concentration in the tissue is an average over the three phases. Furthermore, by introducing partition coefficients, γ_i , for each modelled tissue i , where $\gamma_i = \frac{C_i}{C_{\text{blood}}}$ with C_i being the concentration in tissue i at equilibrium and C_{blood} the concentration in the plasma at equilibrium, the concentration in the blood leaving the tissue i can be estimated as C_i/γ_i .

We apply the blood-flow-limited assumption both in the tumour and the bone marrow. We assume that TAF is produced by tumour cells under hypoxia and that it subsequently enters the blood. In the blood, we assume that TAF is taken up by the bone marrow and that it also decreases due to natural decay, with rate constant r . This decay term also includes uptake of TAF by organs which are not explicitly included in the model, e.g. liver and kidneys. By applying the principle of mass balance in each compartment, we obtain the following ODEs for C_1 , C_2 and C_3 :

$$\frac{d(C_1 V_1)}{dt} = \underbrace{cmH(m - \Gamma v)}_{\text{production}} - \underbrace{q_1 v \left(\frac{C_1}{\gamma_1} - C_2 \right)}_{\text{delivery from tumour}}, \tag{8}$$

$$\frac{d(C_2 V_2)}{dt} = \underbrace{q_1 v \left(\frac{C_1}{\gamma_1} - C_2 \right)}_{\text{delivery from tumour}} - \underbrace{Q_3 \left(C_2 - \frac{C_3}{\gamma_3} \right)}_{\text{delivery from blood}} - \underbrace{r C_2 V_2}_{\text{natural decay}}, \tag{9}$$

$$\frac{d(C_3 V_3)}{dt} = \underbrace{Q_3 \left(C_2 - \frac{C_3}{\gamma_3} \right)}_{\text{delivery from blood}}, \tag{10}$$

where V_2 and V_3 , the volume of blood and bone marrow, respectively, are assumed to be constant and V_1 , due to our flow-limited assumption, is the total tumour tissue volume, i.e.

$$V_1 = m + v. \tag{11}$$

In (9)–(10), we assume that the blood flow to the bone marrow, Q_3 , is constant, whereas in (8)–(9), the blood flow to the tumour is proportional, with constant of proportionality q_1 , to the tumour vasculature, v . In (8), we assume that TAF production is proportional, with constant of proportionality c , to $mH(m - \Gamma v)$, where H is the Heaviside stepfunction ($H(x) = 0$ if $x < 0$ and $H(x) = 1$ if $x \geq 0$). Thus, TAF production by tumour cells occurs only when the ratio m/v exceeds a threshold value, Γ . Since we do not model oxygen explicitly, we regard Γ as an indicator of hypoxic conditions within the tumour. When $m/v > \Gamma$, we suppose that, on average, there are not enough blood vessels to support the tumour mass and that this creates the hypoxic conditions which stimulate the tumour cells to produce TAF. We remark that an alternative form for the TAF production term involves replacing the Heaviside stepfunction by a smooth approximation

$$H(m - \Gamma v) \approx \frac{1}{2} \left(1 + \tanh \left(\frac{m - \Gamma v}{\epsilon} \right) \right), \quad 0 < \epsilon \ll 1, \tag{12}$$

where the Heaviside stepfunction is recovered in the limit as $\epsilon \rightarrow 0$. However, we use the Heaviside function so that we can make analytical progress. Furthermore, when we performed the analysis presented in Section 3 using (12) in place of the Heaviside stepfunction, the qualitative behaviour was unchanged (results not presented).

To summarise, our model comprises 9 ODEs and 2 algebraic relations for 11 dependent variables. Before analysing the model, it is convenient to nondimensionalise and simplify

it by making a quasi-steady assumption in the TAF equations, and thereby eliminating the variables C_i ($i = 1, 2, 3$). The details of these steps are contained in [Appendix A](#). We merely state the final simplified and dimensionless equations in the following subsection.

2.5. Simplified dimensionless equations

From [Appendix A](#), we deduce that, after eliminating the asterisks and the hats in the dimensionless equations, for notational simplicity, the final model equations are:

$$\frac{dx}{dt} = p_1 + p_2mH(m - \Gamma v) - k_1x - k_2mxH(m - \Gamma v) - d_1x, \quad (13)$$

$$\frac{dy}{dt} = k_1x + k_2mxH(m - \Gamma v) - k_3(v + r)myH(m - \Gamma v) - d_2y, \quad (14)$$

$$\frac{dz}{dt} = k_3(v + r)myH(m - \Gamma v) + \frac{p_3(v + r)mzH(m - \Gamma v)}{v} - k_4z - d_3z, \quad (15)$$

$$\frac{du}{dt} = k_4z + \frac{p_5(v + r)muH(m - \Gamma v)}{v} - \frac{\delta_3mu}{m + \delta_4v} - d_5u, \quad (16)$$

$$\frac{dw}{dt} = \frac{p_4(v + r)m(1 + w)H(m - \Gamma v)}{v} - \frac{\delta_1mw}{m + \delta_2v} - d_4w, \quad (17)$$

$$\frac{dm}{dt} = \left(\frac{v}{v + m} - d_0 \right) m, \quad (18)$$

$$v = w + u + 1. \quad (19)$$

3. Angiogenesis and vasculogenesis submodels

Before analysing the full model, we investigate the behaviour of two submodels, in which vessels are formed by either angiogenesis alone or vasculogenesis alone. This will yield insight into whether the two mechanisms for vessel formation lead to different tumour growth dynamics. It will also allow for comparison with the results obtained in Komarova and Mironov (2005).

3.1. Angiogenesis submodel

In this submodel, we assume that the EPCs are not affected by the tumour and that no vessels are formed by vasculogenesis. Thus, we fix $p_2 = k_2 = k_3 = 0$ in (13)–(15) and $z = u = 0$. We assume further that the levels of EPCs in the bone marrow and in the blood are at steady state, and hence that x and y satisfy (see (13)–(14))

$$x = \frac{p_1}{k_1 + d_1} \quad \text{and} \quad y = \frac{k_1 p_1}{d_2(k_1 + d_1)}. \quad (20)$$

This steady state corresponds to the background levels that would exist in the bone marrow and the blood if no tumour were present; it is straightforward to show that the tumour-free steady state is linearly stable to small perturbations in x and y .

Under the above assumptions, our model reduces to (17)–(18), with $v = w + 1$, i.e.

$$\frac{dw}{dt} \equiv W = p_4(w + 1 + r)mH(m - \Gamma(w + 1)) - \frac{\delta_1mw}{m + \delta_2(w + 1)} - d_4w, \tag{21}$$

$$\frac{dm}{dt} \equiv M = \left(\frac{w + 1}{w + 1 + m} - d_0 \right)m. \tag{22}$$

It follows that three types of steady state solutions may arise:

- (i) A trivial steady state:

$$m = w = 0. \tag{23}$$

- (ii) An avascular steady state: If $0 < (\frac{1}{d_0} - 1) < \Gamma$, then no TAF is produced,

$$m = \left(\frac{1}{d_0} - 1 \right) \quad \text{and} \quad w = 0. \tag{24}$$

- (iii) Vascular states: If $(\frac{1}{d_0} - 1) \geq \Gamma$, then TAF production is activated,

$$m = \left(\frac{1}{d_0} - 1 \right)(w + 1) \quad \text{and}$$

$$w^2 + \mathcal{W}w + 1 + r = 0, \tag{25}$$

where

$$\mathcal{W} = \left(2 + r - \frac{\delta_1}{p_4(\frac{1}{d_0} - 1 + \delta_2)} - \frac{d_4}{p_4(\frac{1}{d_0} - 1)} \right), \tag{26}$$

which gives the possibility of two vascular steady states. We see that the existence of physically realistic solutions of (25) requires $\mathcal{W} \leq -\sqrt{4(1+r)}$. This implies that if δ_1 and d_4 (the death terms of the angiogenic vasculature) are relatively small, or p_4 and $1/d_0$ (the proliferation of angiogenic vasculature and tumour) relatively large, then the likelihood of vascular steady states diminishes.

It is clear that the dimensionless parameter $1/d_0$, which represents the ratio of the maximum tumour growth rate to the rate of tumour apoptosis, is the crucial bifurcation parameter. By fixing r, δ_1, p_4, d_4 and δ_2 , we can determine how the steady state solutions change as $1/d_0$ varies. Here we have chosen the fixed parameter values so that the full range of steady state behaviour is realised as $1/d_0$ varies and in so doing we focus on the qualitative behaviour of the model (the values used are stated in Appendix B together with a discussion of realistic parameter ranges). Figure 3 summarises the resulting behaviour.

To determine the local stability of the steady states, we note that for any steady states such that $m \neq \Gamma(w + 1)$, the right-hand sides of (21) and (22) are differentiable with respect to w and m . Therefore, the system is eligible for linear stability analysis (see e.g. Jordan and Smith, 1999). By linearising about each equilibrium point and computing the associated Jacobian matrices, it is straightforward to show that the trivial solution is

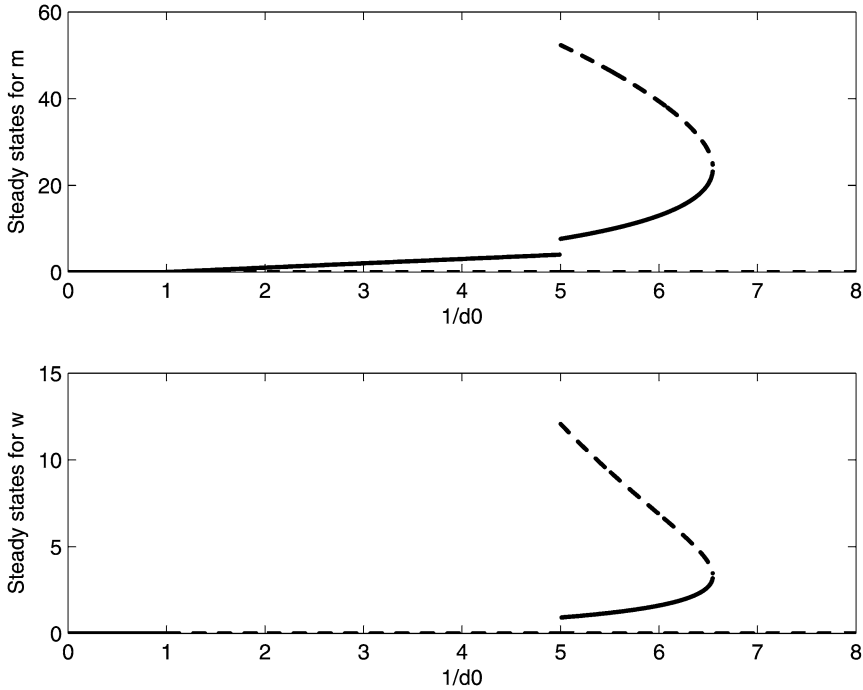


Fig. 3 Bifurcation diagrams showing how the steady state solutions of (21) and (22) change as $1/d_0$ varies. The trivial solution $(m, w) = (0, 0)$ exists for all values of $1/d_0$ and is linearly stable when $1/d_0 < 1$ and unstable otherwise. When $1 < 1/d_0 < \Gamma + 1$, there is a stable avascular steady state (i.e. $w = 0 < m$). Due to the Heaviside term in (21), there is a jump at $1/d_0 = \Gamma + 1$ from the avascular steady state to two vascular steady states, which exist in an interval where $1/d_0 \geq \Gamma + 1$. In this interval, the lower vascular steady states are linearly stable while the upper ones are linearly unstable. For large values of $1/d_0$, the vascular steady states disappear and only the unstable trivial solution exists. Key: solid line: local stability; dashed line: local instability. Parameter values: see Appendix B.

linearly stable if $1/d_0 < 1$ and unstable if $1/d_0 > 1$; i.e., introducing a small tumour into the system will result in tumour decay if $1/d_0 < 1$ and tumour growth if $1/d_0 > 1$. (We note that when $1/d_0 = 1$, the trivial solution is a degenerate critical point.) Similarly, we find that, where it exists, the avascular steady state is linearly stable. For the vascular steady states, the Jacobian, $A = (a_{ij})$, has the following elements:

$$a_{11} \equiv \frac{\partial W}{\partial w} = p_4 \left(\frac{1}{d_0} - 1 \right) (w + 1) - \frac{\delta_1 \left(\frac{1}{d_0} - 1 \right)}{\left(\frac{1}{d_0} - 1 + \delta_2 \right)^2} \left(\frac{1}{d_0} - 1 + \frac{\delta_2}{(w + 1)} \right) - d_4, \tag{27}$$

$$a_{12} \equiv \frac{\partial W}{\partial m} = p_4 (w + 1 + r) - \frac{\delta_1 \delta_2 w}{(w + 1) \left(\frac{1}{d_0} - 1 + \delta_2 \right)^2}, \tag{28}$$

$$a_{21} \equiv \frac{\partial M}{\partial w} = d_0^2 \left(\frac{1}{d_0} - 1 \right)^2, \tag{29}$$

$$a_{22} \equiv \frac{\partial M}{\partial m} = -d_0^2 \left(\frac{1}{d_0} - 1 \right), \quad (30)$$

with w specified by (25). For linear stability in this case, we require the eigenvalues λ of A to satisfy $\text{Re}(\lambda) < 0$, i.e. $\text{tr}(A) = a_{11} + a_{22} < 0 < \det(A) = a_{11}a_{22} - a_{12}a_{21} \equiv D$. By setting $D = 0$ and solving for w , we conclude that the determinant of A only vanishes at $w = -\mathcal{W}/2 \equiv \bar{w}$ corresponding to the double root of Eq. (25). Furthermore, along the curve in $(w, 1/d_0)$ -space given by Eq. (25), we have

$$\frac{\partial D}{\partial w} = \frac{\partial D}{\partial w} + \frac{\partial D}{\partial(1/d_0)} \frac{\partial(1/d_0)}{\partial w} = -2p_4(1/d_0 - 1)^2 d_0^2 + \frac{\partial D}{\partial(1/d_0)} \frac{\partial(1/d_0)}{\partial w}, \quad (31)$$

where $\frac{\partial(1/d_0)}{\partial w}$ can be obtained implicitly from (25) and shown to satisfy $\frac{\partial(1/d_0)}{\partial w} \Big|_{\bar{w}} = 0$. Thus, it follows that

$$\frac{\partial D}{\partial w} \Big|_{\bar{w}} = -2p_4(1/d_0 - 1)^2 d_0^2 < 0, \quad (32)$$

which, together with the fact that $D = 0$, if and only if $w = \bar{w}$, indicates that $D > 0$ on the lower branch, where $w = \bar{w} - \sqrt{\bar{w}^2 - (1+r)}$, and $D < 0$ on the upper branch, where $w = \bar{w} + \sqrt{\bar{w}^2 - (1+r)}$. Thus, the lower branch is stable provided that $\text{tr}(A) < 0$. In fact, this is always the case since $a_{11} < 0$ and $a_{22} = -d_0^2(1/d_0 - 1) < 0$ (see (30)). To determine that $a_{11} < 0$, we investigate the qualitative behaviour of the w -nullcline (from (21)) and the m -nullcline (from (22)), and deduce that the sign of W must change from positive to negative, as we go along a line which is parallel to the w -axis and crosses the w -nullcline at the first steady state (see e.g. Murray, 1993), i.e. $a_{11} \equiv \frac{\partial W}{\partial w} < 0$. Regarding the steady states on the upper branch, we note that they always correspond to saddles, because the eigenvalues are real and of opposite signs.

To illustrate the range of behaviours that can occur, we compute phase planes and numerical solutions to the model equations. We suppose that initially $w = 0 < m$, in which case the tumour must rely on the background vasculature for its initial nutrient supply. This corresponds to implanting into a tissue an avascular tumour of size $m > 0$ at $t = 0$ or possibly to monitoring an avascular tumour that developed previously (for $t < 0$). We integrate Eqs. (21)–(22) numerically using a Runge–Kutta method (MATLAB's ODE solvers).

A typical phase plane illustrating the behaviour when there are two vascular steady states is presented in Fig. 4. Dependent on the initial tumour size, three qualitatively different types of behaviour are observed. When the initial tumour is small, it undergoes avascular growth in response to the existing vasculature (see trajectory with initial condition $w(0) = 0, m(0) = 2$). TAF production and angiogenesis switch on when the vascular density $v/m = (w + 1)/m$ decreases to $1/\Gamma$. As m and w further increase, angiogenesis slows down due to increased occlusion and apoptosis of the vessels. This causes the vascular density to drop (as the trajectory meets the w -nullcline) and the tumour evolves to the stable vascular equilibrium. If the initial tumour is intermediate-sized (e.g. $m(0) = 30$) then the tumour produces angiogenic factors immediately (since $(w + 1)/m < 1/\Gamma$). However, in spite of new vessel growth, the tumour volume still decreases. This is because the angiogenic response is insufficient to sustain the tumour, i.e. the resulting vascular density is such that the tumour cell proliferation rate is smaller than the rate of

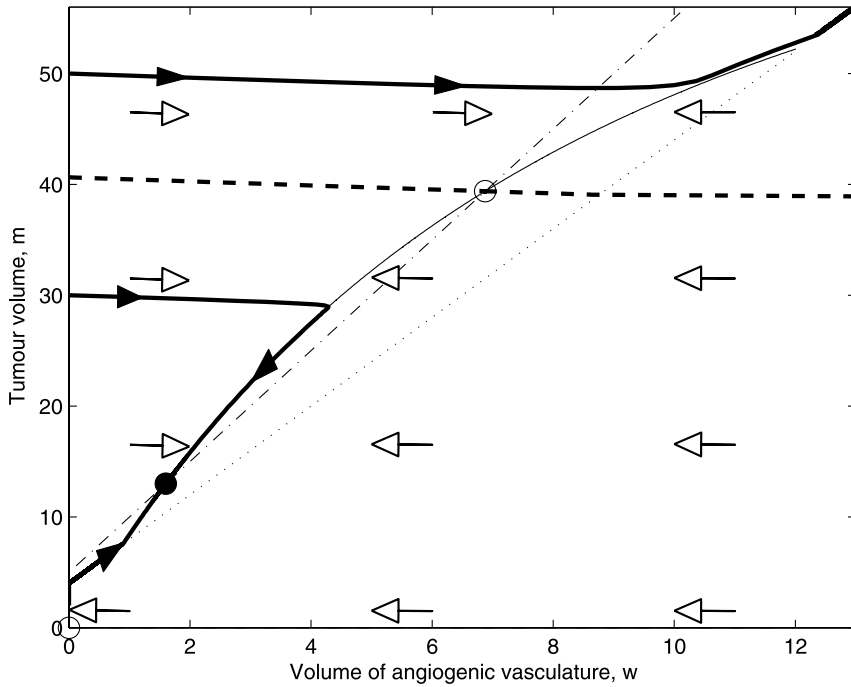


Fig. 4 (w, m) -phase plane diagram illustrating the behaviour of our angiogenesis submodel (Eqs. (21)–(22)) when there are three steady state solutions: an unstable trivial solution, a locally stable vascularised solution and an unstable vascularised solution. Three trajectories are presented showing how the initial size of the tumour affects its evolution. For small tumours (e.g. $m(0) = 2$), the tumour undergoes a transient period of avascular growth until it becomes large enough to stimulate an angiogenic response. Thereafter, the tumour evolves to the stable vascular state. For intermediate-sized tumours (e.g. $m(0) = 30$), the tumour is large enough to elicit an angiogenic response immediately. Its volume, m , decreases slowly compared to the vasculature until the system meets the w -nullcline and enters the basin of attraction of the stable vascular steady state. For larger-sized tumours (e.g. $m(0) = 50$), unbounded growth ensues. Key: dashed-dotted lines: m -nullclines; solid lines: w -nullclines; dotted line: line above which TAF production is active; open circles: linearly unstable steady states; closed circle: linearly stable steady state; bold lines with solid arrows: trajectories for three choices of initial conditions; bold dashed line: separatrix dividing the phase plane into different areas, here regions of unbounded and bounded growth. Parameter values: according to [Appendix B](#) with $1/d_0 = 6$.

apoptosis. When the vasculature starts to decrease due to occlusion and apoptosis, the tumour evolves to the stable vascular equilibrium. In contrast, an initially large tumour mass (e.g. $m(0) = 50$) induces a stronger angiogenic response, which enables the tumour to undergo unbounded growth. We note here that, consistent with our model's bifurcation structure, it has been shown experimentally, in Ke et al. (2000), that tumour growth depends on the angiogenic phenotype. Upon implantation of different glioma cell lines, the tumour volume remained constant or decreased for cell lines that were less angiogenic (i.e. secreted low amounts of VEGF), while tumour types of higher angiogenic capacity increased rapidly in size (Ke et al., 2000).

In Fig. 4, we see that when the tumour grows unboundedly, $(w + 1)/m \rightarrow 1/\Gamma$. This will always be the case when growth is unbounded, because if m and w are sufficiently large in the region of TAF production, then $dw/dt \gg dm/dt$ (from (21) and (22) we note that the growth term in (21) is dominant when m and w are large). This will ultimately cause the vector field dm/dw to become horizontal, and point toward the curve $m = \Gamma(w + 1)$, which we henceforth term the discontinuity boundary. On the other hand, where $m < \Gamma(w + 1)$, the vector field always points in the opposite direction since $dw/dt < 0$ and $dm/dt > 0$. As a result, any trajectory which hits the boundary cannot leave it. This corresponds to so-called “sliding” on the discontinuity boundary (di Bernardo et al., 2005; Leine et al., 2000).

In order to determine how solutions evolve on the discontinuity boundary, we exploit the fact that (21) has a discontinuous right-hand side to write Eqs. (21) and (22) as a Filippov system (di Bernardo et al., 2005; Leine et al., 2000):

$$\frac{dx}{dt} = \begin{cases} f_1 & \text{if } h > 0, \\ f_2 & \text{if } h < 0, \end{cases} \quad (33)$$

where $x = (w, m)$,

$$f_1 = \left[p_4(w + 1 + r)m - \frac{\delta_1 m w}{m + \delta_2(w + 1)} - d_4 w, \frac{(w + 1)m}{(w + 1) + m} - d_0 m \right], \quad (34)$$

$$f_2 = \left[-\frac{\delta_1 m w}{m + \delta_2(w + 1)} - d_4 w, \frac{(w + 1)m}{(w + 1) + m} - d_0 m \right] \quad (35)$$

and $h = m - \Gamma(w + 1)$, so that $h = 0$ is the discontinuity boundary. The vector $f = (\dot{w}, \dot{m})|_{h=0}$ is given by

$$f = \alpha f_1 + (1 - \alpha) f_2, \quad \text{where } 0 \leq \alpha = \frac{\text{proj}_n f_2}{\text{proj}_n (f_2 - f_1)} \leq 1 \quad (36)$$

and $\text{proj}_n f_2$ is the projection of f_2 onto the normal, $n = \nabla h = (-\Gamma, 1)$, to the discontinuity boundary. In our case, the time derivative on the switching boundary becomes

$$\begin{aligned} f &= \left(\frac{1}{\Gamma} \left[\frac{(w + 1)}{(w + 1) + m} - d_0 \right] m, \left[\frac{(w + 1)}{(w + 1) + m} - d_0 \right] m \right) \\ &= \left[\frac{1}{1 + \Gamma} - d_0 \right] ((w + 1), m). \end{aligned} \quad (37)$$

Thus, on the switching manifold, m and w grow exponentially with rate $1/(1 + \Gamma) - d_0$, provided that the nullcline of m lies above the switching boundary, i.e. $1/d_0 > \Gamma + 1$.

3.2. Vasculogenesis submodel

If we assume vasculogenesis is dominant, then $p_4 = w = 0$ in (17) and our model reduces to Eqs. (13)–(16) and (18) with $v = u + 1$. There may be the following steady state solutions:

(i) A trivial steady state:

$$m = 0, \quad u = 0, \quad z = 0, \quad y = \frac{k_1 p_1}{d_2(k_1 + d_1)} \quad \text{and} \quad x = \frac{p_1}{k_1 + d_1}. \quad (38)$$

The levels of EPCs in the bone marrow and blood correspond to the natural background levels.

(ii) An avascular steady state: If $0 < (\frac{1}{d_0} - 1) < \Gamma$, then no TAF is produced,

$$m = \left(\frac{1}{d_0} - 1\right), \quad u = 0, \quad z = 0, \quad y = \frac{k_1 p_1}{d_2(k_1 + d_1)} \quad \text{and} \\ x = \frac{p_1}{k_1 + d_1}. \quad (39)$$

As for the trivial steady state, the levels of EPCs in the bone marrow and blood are at the natural background levels.

(iii) Vascular steady states: If $(\frac{1}{d_0} - 1) \geq \Gamma$, then there is active TAF production and we have:

$$m = \left(\frac{1}{d_0} - 1\right)(u + 1), \quad x = \frac{p_1 + p_2 m}{k_1 + k_2 m + d_1}, \\ y = \frac{[k_1 + k_2 m]x}{k_3(u + 1 + r)m + d_2}, \quad (40)$$

$$z = \frac{k_3(u + 1)(u + 1 + r)m y}{(k_4 + d_3)(u + 1) - p_3(u + 1 + r)m}, \quad (41)$$

where u satisfies a sixth-order polynomial:

$$\tilde{f}(u) = g(u) - f(u) = 0, \quad (42)$$

with

$$g(u) = p_5 p_3 k_3 k_2 \left(\frac{1}{d_0} - 1\right)^4 u \prod_{i=1}^5 (u - G_i), \quad (43)$$

$$G_1 = \frac{1}{p_5(\frac{1}{d_0} - 1)} \left(\frac{\delta_3(\frac{1}{d_0} - 1)}{\frac{1}{d_0} - 1 + \delta_4} + d_5 \right) - (1 + r), \\ G_2 = \frac{k_4 + d_3}{p_3(\frac{1}{d_0} - 1)} - (1 + r), \quad (44)$$

$$G_{3,4} = -\frac{(2+r)}{2} \pm \frac{\sqrt{(2+r)^2 - 4(1+r + \frac{d_2}{k_3(\frac{1}{d_0} - 1)})}}{2}, \\ G_5 = \frac{-k_1 - d_1}{k_2(\frac{1}{d_0} - 1)} - 1, \quad (45)$$

$$f(u) = k_4 k_3 k_2 p_2 \left(\frac{1}{d_0} - 1 \right)^3 \prod_{i=1}^4 (u - F_i), \quad (46)$$

$$F_1 = -(1+r), \quad F_2 = -1, \quad F_3 = \frac{-k_1}{k_2 \left(\frac{1}{d_0} - 1 \right)} - 1 \quad \text{and} \\ F_4 = \frac{-p_1}{p_2 \left(\frac{1}{d_0} - 1 \right)} - 1. \quad (47)$$

It is possible to show that (42) has at most two physically realistic vascular solutions and that their existence depends on the sign of the zeros of (43) (see Appendix C for details).

As for the angiogenesis submodel, linear stability analysis reveals that the trivial solution is stable if $1/d_0 < 1$ (and unstable otherwise), and that the avascular solution is locally stable where it exists. The stability of the vascular steady state solutions was determined using the dynamical systems package XPPAUT (Ermentrout, 2002). Numerical simulations using a wide range of parameter values suggest that the bifurcation structure of the vasculogenesis submodel is similar to that for the angiogenesis submodel (shown in Fig. 3). In particular, where they exist, vascular steady states on the upper branch are unstable while those on the lower branch are locally stable.

4. Full model

Based on the analysis of the angiogenesis and vasculogenesis submodels, we conclude that similar steady states and bifurcations are exhibited by tumours in which either angiogenesis or vasculogenesis dominates. To see whether the bifurcation structure is the same when both vascularisation mechanisms are active, we analysed the full model, consisting of Eqs. (13)–(19). Our analysis shows that a trivial steady state solution always exists, satisfying (38) and $w = 0$. As in the submodels, the tumour-free steady state solution is linearly stable if $1/d_0 < 1$ (and unstable otherwise). Furthermore, depending on whether $(\frac{1}{d_0} - 1) < \Gamma$, avascular or vascular steady states can occur. The avascular steady state solution, which satisfies (39) and $w = 0$, is linearly stable. As for the vasculogenic submodel, to characterise the vascular steady states, we explored the full model numerically for a range of parameter values. We always obtained bifurcation diagrams similar in form to Fig. 3, which suggests that the bifurcation structure for the submodels is preserved when angiogenesis and vasculogenesis occur simultaneously.

Motivated by the seemingly contradictory reports on both the extent of vasculogenesis in tumours and its impact on tumour growth rate, in the remainder of this section, we investigate its importance as the tumour either evolves to a vascular steady state or undergoes unbounded growth. We calculate the proportion of vasculogenic neovascularity, $PVN = u/(w + u)$, and use it to characterise a vascular tumour as vasculogenic if $PVN > 0.5$ and angiogenic otherwise. We also examine how the combination of angiogenesis and vasculogenesis affects the tumour's overall growth rate. Furthermore, we establish how the degree of vasculogenesis and its effect on tumour growth change as certain selected model parameters are varied.

In Fig. 5, we present results for a simulation in which the tumour undergoes unbounded growth. Where possible, we have chosen realistic parameter values (see Appendix B for a discussion); other values were chosen so that the resulting (dimensional) level of TAF (VEGF) in the blood, C_2 , and the proportion of vasculogenic neovasculature, PVN , are similar over time to those reported in Spring et al. (2005) for hepatocellular carcinoma in Alb-Tag mice (where tumour growth was monitored over a period of 16 weeks). We note that the initial contribution from vasculogenesis is low, a result which is consistent with the observations in Spring et al. (2005) where the proportion of EPC-derived vasculature increased from approximately 3% at week 10 to 28% at week 16 (in Fig. 5 corresponding to time points 49 and 78, respectively). From Fig. 5, we note also that the level of EPCs in the blood, y (which was not given in Spring et al. (2005)), at first increases due to the increasing level of TAF in the blood (as for example observed in burn and vascular trauma patients, where the blood level of EPCs reflects the circulatory level of VEGF (Gill et al., 2001)). However, over time, as tumour growth advances, y reaches a maximum value before dropping to low levels (here the maximum corresponds to a dimensional value of roughly 4500 cells/ml, comparable to levels seen in cancer patients (Dome et al., 2006)). The decrease in y over time occurs because as the tumour and the vasculature grow unboundedly, the adherence term (with coefficient k_3) ultimately becomes dominant in the y -equation (14), corroborating theoretical predictions in Komarova and Mironov (2005) that the level of EPCs in the blood will decline at large times. In Komarova and Mironov (2005), the drop in circulating EPCs was accompanied by a drop in the level of EPCs in the bone marrow, x , and a decrease in the contribution from vasculogenesis at large times. However, these features are not present in our model (as evident from Fig. 5) due to our assumption that the EPCs may proliferate in response to TAF both within the bone marrow and the tumour. Thus, in our model low levels of EPCs in the blood may not be an indicator of low vasculogenesis, but instead an indicator of their relatively short transit time in the bloodstream, i.e. rapid adherence at the tumour site.

In Fig. 6, we show how, in cases for which the tumour grows unboundedly, the inclusion of vasculogenesis increases its growth rate and affects its growth dynamics compared to cases for which only angiogenesis is active. We do this by varying p_3 , the proliferation rate of the EPCs, and k_4 , the rate at which EPCs form vessels. The initial conditions are chosen so that the tumour is avascular but large enough that it starts producing TAF immediately (thus the system initially evolves on the discontinuity boundary). Due to increased occlusion and apoptosis, over time the vascular density falls in all cases. However, the inclusion of vasculogenesis leads to higher vascular densities, and therefore increased tumour growth. When p_3 is high ($p_3 = 0.002$), the vasculogenic response is slower when k_4 is small ($k_4 = 0.001$) than when it is large ($k_4 = 0.5$); note that initially PVN is smaller. However, with k_4 small, the effect of vasculogenesis on the tumour's long-term growth rate is stronger. This is because a small value of k_4 allows EPCs to accumulate within the tumour, and subsequently this population of EPCs expands due to rapid proliferation in response to TAF. Thus, the level of EPCs increases to high values, and vasculogenesis outstrips angiogenesis ($PVN \rightarrow 1$). By contrast, if p_3 is small ($p_3 = 0.0002$), then the tumour is less vasculogenic. In this case, the tumour's growth rate is affected more if k_4 is high ($k_4 = 0.5$); when both k_4 and p_3 are small ($k_4 = 0.001$ and $p_3 = 0.0002$) the PVN is low and the tumour's growth rate does not change markedly (on this time scale) when vasculogenesis is included (simulation not presented).

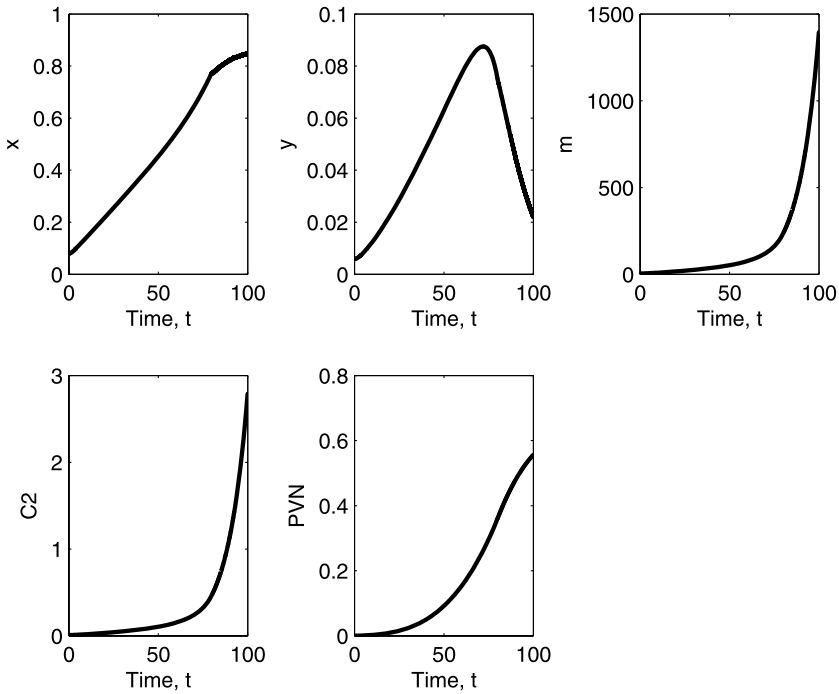


Fig. 5 Series of curves (solutions of (13)–(19)) showing how, in the case of unbounded growth, the level of EPCs in the bone marrow, x , the level of EPCs in the blood, y , the tumour volume, m , the level of TAF in the blood, C_2 , and the proportion of vasculogenic vasculature, PVN , evolve over time. We observe that the contribution from vasculogenesis becomes more pronounced at large times. The level of EPCs in the blood, y , first reflects the level of TAF in the blood. With time y reaches a maximum and then drops to low levels, in contrast to x which rises and remains at an elevated level. Parameter values: see Appendix B. In these simulations $1/d_0 = 9$. The initial conditions are: $m = 4$, $u = 0$, $w = 0$, $z = 0$, $y = 3/520$ and $x = 1/13$ at $t = 0$.

We remark that since on the discontinuity boundary the vascular density attains the largest value possible for the tumour to still produce angiogenic factors, it corresponds to the maximum possible growth rate of a vascularised tumour. By increasing the proliferation rate and decreasing the occlusion rate of the angiogenic vessels, we obtained cases where the inclusion of vasculogenic vasculature did not noticeably increase the tumour growth rate. In these cases, angiogenesis was so strong that the tumour vascularisation took place exclusively on the discontinuity boundary, and the extra vasculogenesis-derived vasculature did not have an impact. We also note that this works both ways, i.e. if vasculogenesis is strong enough then adding angiogenesis may not have a perceivable impact.

We end this section by showing in Fig. 7 where in (p_4, p_3) -space and (p_4, k_3) -space vascular steady states exist (in the shaded regions) and how the total vasculature, v , and the PVN associated with the stable vascular steady state vary with p_3 and p_4 (panels A and B, respectively) and with k_3 and p_4 (panels C and D, respectively). The parameter p_3 relates to EPC proliferation, k_3 to the rate of EPC adhesion to the vessel wall

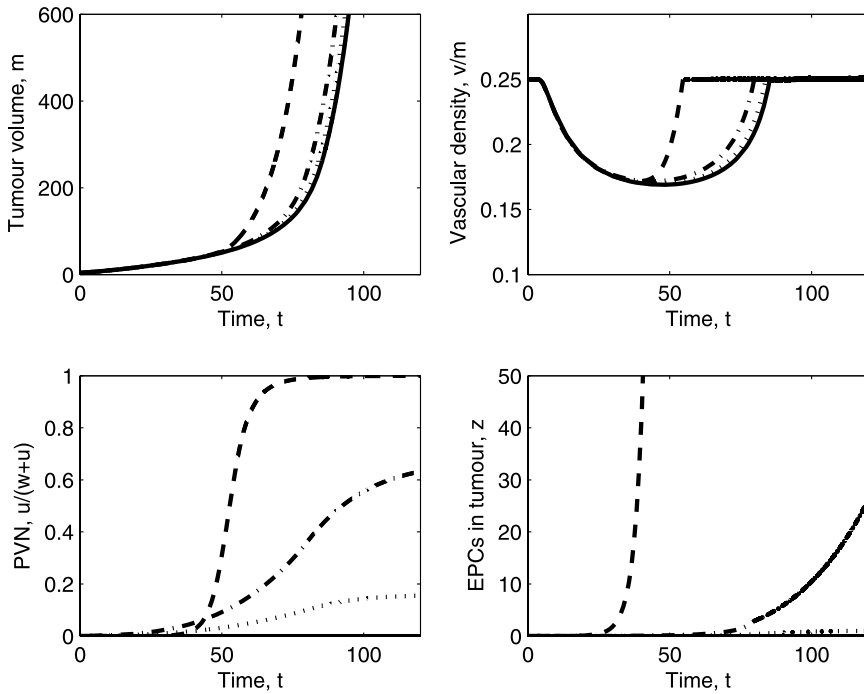


Fig. 6 Series of curves (solutions of (13)–(19)) showing how, in the case of unbounded growth, varying the vasculogenic response by altering the rate of EPC proliferation, p_3 , and the rate of EPC vessel formation, k_4 , influences tumour volume, m , vascular density, v/m , proportion vasculogenic neovasculature, PVN , $u/(w+u)$, and number of EPCs in the tumour, z . For comparison, a case where only angiogenesis is active is also presented (solid line in each panel). We observe that when both angiogenesis and vasculogenesis contribute to the vasculature, then the tumour grows larger than in the case with angiogenesis only. The increase in tumour volume occurs because the inclusion of vasculogenesis results in higher vascular densities. When both p_3 and k_4 are large (dashed-dotted line), vasculogenic vessels form more rapidly, resulting in the highest PVN initially. However, if p_3 is large while k_4 is small (dashed line), vasculogenesis ultimately dominates with $PVN \rightarrow 1$. In this case, the number of EPCs increases to high levels. If p_3 is small and k_4 large (dotted line), then the level of vasculogenesis is always low and the effect on tumour volume is minimal. Key: solid line: angiogenesis only; dotted line: angiogenesis and vasculogenesis with $(k_4, p_3) = (0.5, 0.0002)$; dashed-dotted line: angiogenesis and vasculogenesis with $(k_4, p_3) = (0.5, 0.002)$; dashed line: angiogenesis and vasculogenesis with $(k_4, p_3) = (0.001, 0.002)$. Parameter values: see Appendix B, with $p_2 = k_2 = k_3 = 0$ for the angiogenesis-only case. In these simulations $1/d_0 = 9$ which corresponds to unbounded growth for all cases. The initial conditions are: $m = 4$, $u = 0$, $w = 0$, $z = 0$, $y = 3/520$ and $x = 1/13$ at $t = 0$.

and p_4 to EC proliferation. We see that for a fixed value of p_3 , increasing p_4 increases the total vasculature, v , at the steady state (panel A). A similar increase in v is obtained if, for a fixed value of p_4 , p_3 increases. Since $m = (\frac{1}{d_0} - 1)v$ at the steady state, this also leads to an increase in tumour volume. Therefore, when vasculogenesis and angiogenesis act simultaneously, the tumour grows to a larger equilibrium size than when either vasculogenesis or angiogenesis act in isolation. We also note that if these parameters exceed threshold values, then the steady states are lost and unbounded growth ensues. This means

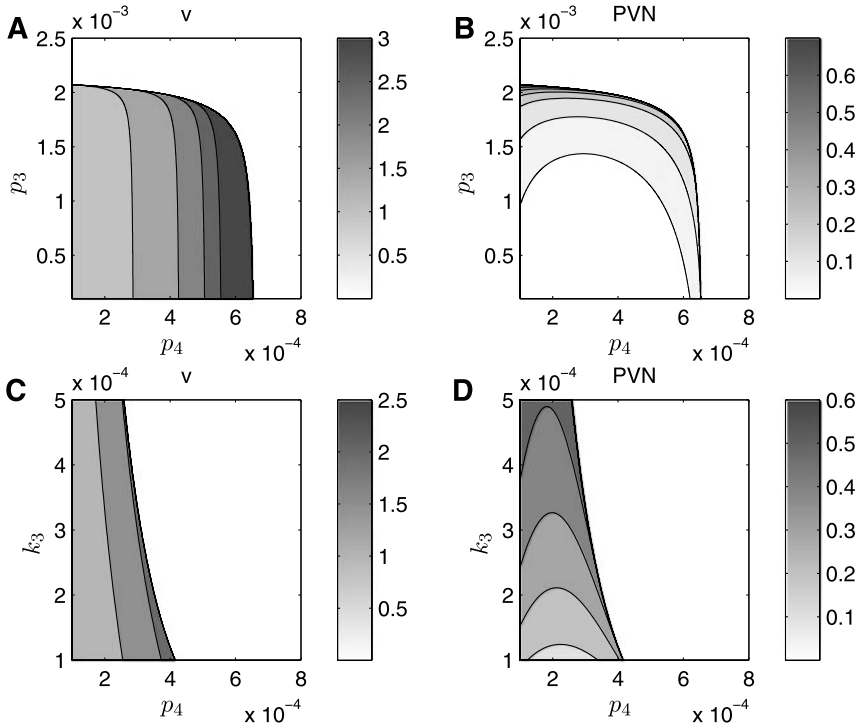


Fig. 7 Two sets of bifurcation diagrams showing how at the stable vascular steady state the total vasculature (left panels) and the proportion vasculogenic neovasculature (right panels) vary as either p_3 and p_4 or k_3 and p_4 are varied. Here, white areas correspond to unbounded vascular growth; thus, if the parameters exceed threshold values, the vascular steady states are lost. (A, B) Panel A shows that as the rate of EPC proliferation, p_3 , and the rate of EC proliferation, p_4 , increase, the total vasculature, v , increases at the steady state. In panel B, the proportion vasculogenic neovasculature, PVN , is largest when p_3 is large and p_4 small. (C, D) An increase in the rate of EPC adhesion, k_3 , or the rate of EC proliferation, p_4 , leads to additional vasculature at the stable steady state (panel C), with vasculogenesis dominating ($PVN > 0.5$) for large k_3 and small p_4 (panel D). Parameter values: as in Appendix B, with $1/d_0 = 6$. In these simulations we also fix $p_5 = p_4$.

that the addition of extra vasculature due to vasculogenesis (or angiogenesis) could cause a previously stable vascular tumour to undergo unbounded growth.

Regarding the proportion of vasculogenesis-derived vessels, we observe that it is largest when p_3 is high and p_4 low (Fig. 7, panel B). Interestingly, for a fixed value of p_3 , PVN first decreases as p_4 increases and then increases; thus PVN is lowest for intermediate values of p_4 . An increase in p_4 initially affects angiogenesis more than vasculogenesis; this is because the proliferation of the background vasculature produces only angiogenic vessels (compare the terms with coefficients p_4 and p_5 in (17) and (16), respectively). As p_4 is increased further, however, the relative contribution from vasculogenesis increases since the increase in p_4 causes an increase in v and m , which enhances the proliferation of z until, for p_4 sufficiently large, vasculogenesis exceeds angiogenesis (see the term with coefficient k_4 in (16)). This is consistent with the behaviour described above for the case of unbounded growth that suggests that vasculogenesis becomes more dominant as

tumour growth accelerates. In Fig. 7, we note that trends similar to those described above occur when k_3 is varied with p_4 (see panels C and D). We remark here that in Fig. 7, we fix $p_4 = p_5$, however, qualitatively similar observations hold when $p_4 \neq p_5$ and only p_4 is varied.

4.1. Therapeutic implications

Below we discuss general treatment strategies, focusing on qualitative behaviour rather than the precise details associated with a particular therapy. In general, chemotherapy acts on the tumour directly by killing proliferating tumour cells, while anti-angiogenic treatments act indirectly by inhibiting the growth of new vasculature.

The affected model parameter in the case of chemotherapy is $1/d_0$, i.e. the ratio of the maximum tumour proliferation rate to the tumour cell apoptosis rate. From the bifurcation diagrams, presented in Fig. 3, we conclude that as $1/d_0$ decreases tumour growth is inhibited. In particular, we note that if $1/d_0$ is low enough, then the tumour will be eradicated, or persist in an avascular state. An effective treatment strategy could therefore involve applying a drug which decreases $1/d_0$ by increasing the tumour apoptosis rate. In Fig. 8, two different chemotherapy protocols are applied to a vascularised tumour which initially grows unboundedly ($1/d_0 = 9$). While a single dose of chemotherapy temporarily inhibits tumour growth, unbounded growth resumes once $1/d_0$ returns to its initial value, corresponding to treatment being stopped (Fig. 8, panels A and B). To maintain the tumour in an avascular state, the treatment must be continued. Alternatively, if the tumour is continuously infused with a weaker drug or a lower dose (corresponding to a higher value of $1/d_0$), then the tumour may be managed as a small vascularised mass (see Fig. 8, panels C and D). If the lower strength dose is given initially, however, this has a negligible inhibitory effect; the tumour undergoes monotonic expansion (results not presented).

When simulating therapies that target the vasculature, the way in which the anti-angiogenic drug acts determines which model parameters should be altered. Consider, for example, a toxin such as VEGF-A121-DT385 conjugate, which inhibits EC proliferation by binding to the VEGF-receptor VEGFR-2 (Hoeben et al., 2004). In our model, such behaviour can be achieved by reducing the parameters p_4 and p_5 . If we assume that the therapy has the same effect on EPCs, which are also VEGFR-2-positive (Stoll et al., 2003), then the parameter p_3 would also be reduced. Alternative approaches involve inhibiting EC migration by targeting integrins, such as $\alpha_v\beta_3$ and $\alpha_v\beta_5$ (Stoll et al., 2003), or decreasing the tumour secretion of VEGF, which, according to Hoeben et al. (2004), is how the agent Rapamycin acts. In our model, the latter approach corresponds to reducing the dimensional parameter c , and therefore the dimensionless parameter groupings k_2 , k_3 , p_2 , p_3 , p_4 and p_5 (see Appendix (A.25)). Alternatively, the level of active TAF could be reduced by introducing an antibody which blocks VEGF's binding to its receptors (Hoeben et al., 2004; Stoll et al., 2003). In Fig. 9, we contrast the treatment outcome if only EC proliferation is targeted with a case targeting only EPC proliferation as well as a case of a combination treatment inhibiting TAF production. We model the different situations by decreasing the relevant parameters to 10% of their initial value while treatment is being administered. Figure 9 (panel A) shows that if the tumour has a relatively high EPC proliferation rate and a low EC proliferation rate, then targeting only ECs is ineffective, whereas targeting only EPCs is almost as effective as the combination treatment. The opposite holds true if the tumour has a relatively low EPC proliferation rate and a

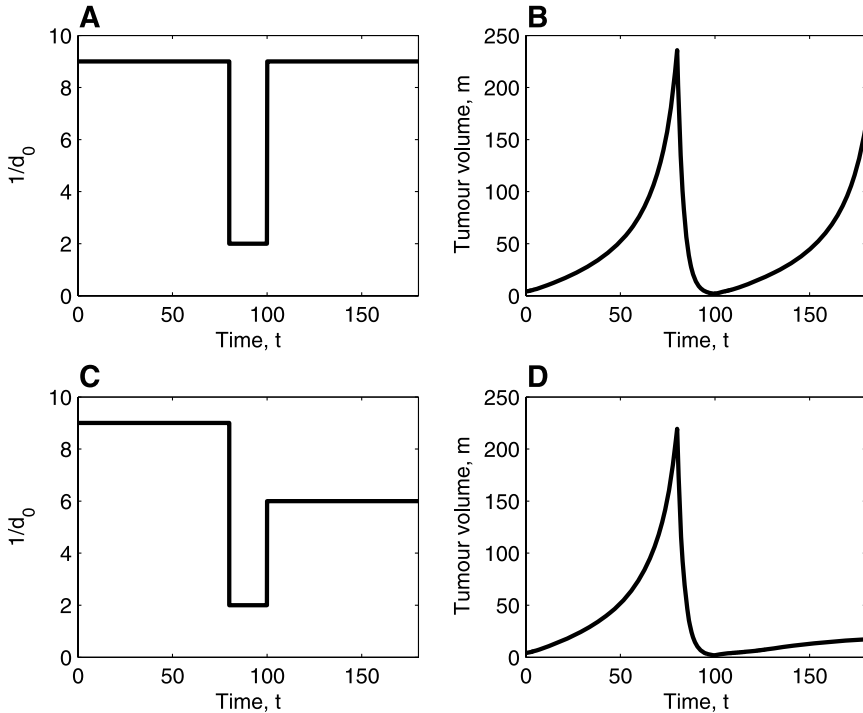


Fig. 8 Two sets of simulations (of (13)–(19)) showing how the tumour volume (right panels) is affected by two different chemotherapy protocols (left panels). The chemotherapy reduces $1/d_0$ in the manner presented by inducing tumour cell apoptosis. As a result the tumour’s short- and long-term growth dynamics change. (A, B) In this case therapy is applied for $80 < t < 100$ after which the tumour resumes unbounded growth. (C, D) By applying a second, lower strength, dose (with a higher value of $1/d_0$) directly after the first drug (i.e. for $100 < t < 180$) the tumour evolves to a stable vascularised steady state at large times. Parameter values: as in Appendix B, with $1/d_0 = 9$. In both cases, we fix $m = 4$, $u = 0$, $w = 0$, $z = 0$, $y = 3/520$ and $x = 1/13$ at $t = 0$.

high EC proliferation rate (Fig. 9, panel C). Furthermore, if both EC and EPC proliferation are strong (Fig. 9, panel B), then the individual treatments are ineffective compared to the combination treatment. These therapy outcomes are consistent with the bifurcation diagram presented in Fig. 10. From Fig. 10, it is clear that for a tumour with a large value of p_3 and a small value of p_4 (point marked by a lowercase a in Fig. 10), a therapy which reduces only p_4 will have little effect on the tumour growth rate since no steady state is induced (the tumour will continue to undergo unbounded vascular growth). By contrast, if the tumour has a small value of p_3 and a large value of p_4 (point c in Fig. 10), then only a treatment that decreases p_4 may halt the tumour growth. Finally, if the rates of EC and EPC proliferation are both high (point b in Fig. 10), a steady state is only achieved by targeting both p_3 and p_4 , i.e. individual treatments will not be as effective as a combination treatment. We also remark that if started too late (i.e. when the tumour is large), then the therapies may be less effective since the tumour may have outgrown the basin of

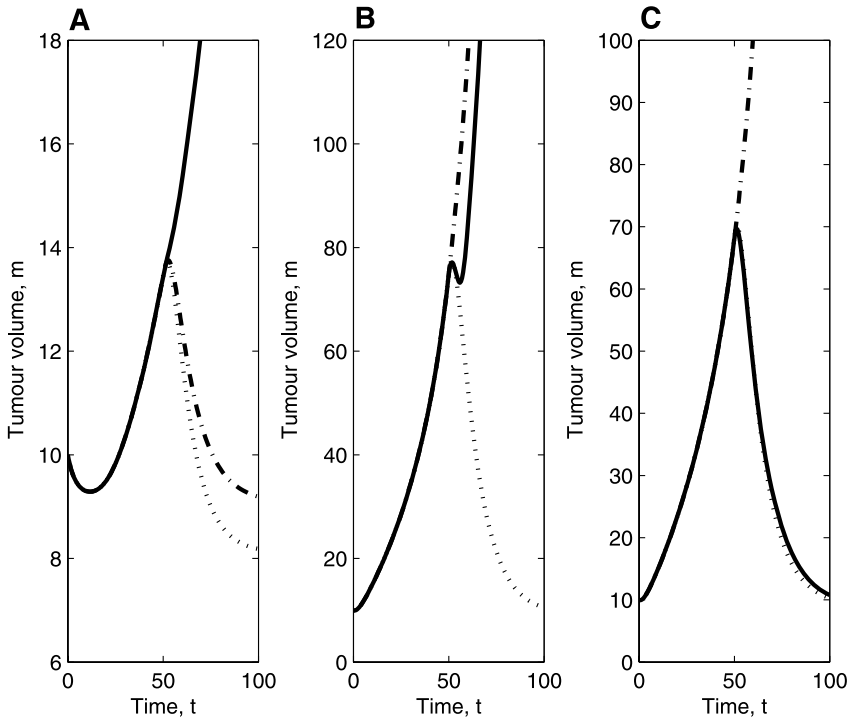


Fig. 9 Series of simulations (of (13)–(19)) showing how the tumour’s response to different vasculature-targeting therapies depends on the model parameters p_3 and p_4 that relate to EPC and EC proliferation, respectively. (A) For a tumour which is growing unboundedly with a relatively high EPC proliferation rate and relatively low EC proliferation rate ($p_3 = 0.0025$ and $p_4 = 0.0001$, corresponding to point a in Fig. 10), targeting only EC proliferation (solid line) is ineffective, compared to targeting only EPC (dashed-dotted line) and inhibiting TAF production (dotted line). (B) For a tumour which has relatively high EPC and EC proliferation rates ($p_3 = 0.0025$ and $p_4 = 0.001$, corresponding to point b in Fig. 10), only the combination treatment which reduces TAF production inhibits tumour growth effectively. (C) When the EC proliferation rate is high while the EPC proliferation is low ($p_3 = 0.0008$ and $p_4 = 0.001$, corresponding to point c in Fig. 10), the treatment that only affects EC proliferation is sufficient to inhibit tumour growth, while, contrary to (A), targeting only EPCs is not. Key: solid line: targeting only EC proliferation; dashed-dotted line: targeting only EPC proliferation; dotted line: inhibiting TAF production. Parameter values: as in Appendix B with $1/d_0 = 9$. During treatment, i.e. for $t > 50$, the affected parameters are reduced to 10% of their normal values. For all cases, the initial conditions are: $m = 12$, $u = 0$, $w = 0$, $z = 0$, $y = 3/520$ and $x = 1/13$ at $t = 0$.

attraction for the steady state; in this case the tumour will continue to grow exponentially when treatment is applied.

5. Discussion

We have developed an ODE model which describes how a tumour can become vascularised by angiogenesis and vasculogenesis and, compared to earlier models (Komarova and Mironov, 2005; Stoll et al., 2003), includes some additional characteristics of tumour

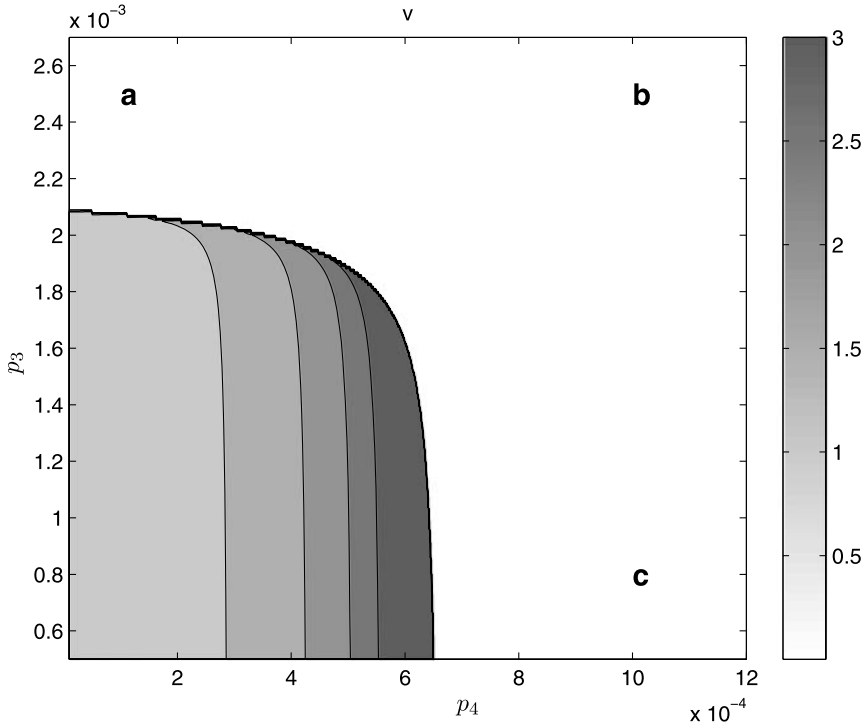


Fig. 10 Bifurcation diagram showing where in (p_4, p_3) -space vascular steady states exist (in the shaded regions) and, where they do, how the total vasculature, v , associated with the stable vascular steady state changes with p_3 and p_4 . The diagram suggests that for a tumour which is growing unboundedly with a relatively high EPC proliferation rate and low EC proliferation rate (point marked a), anti-vascular therapy should focus mainly on decreasing EPC proliferation, since the only possible way to obtain a stable steady state from this point is by decreasing p_3 . The opposite applies for a tumour with a high value of p_4 and a low value of p_3 (point marked c); here only a lower value of p_4 may introduce a steady state. If the rates of EPC and EC proliferation both are high (point marked b), then a steady state can only be achieved by lowering both parameters. Parameter values: as in Appendix B, with $1/d_0 = 9$. In these simulations, we also fix $p_5 = p_4$.

growth. An important new feature is our assumption that the vascular density, v/m , is an indicator of hypoxia within the tumour, and thus, correlates with TAF production; in our model TAF production is activated only if the vascular density drops below a certain threshold value. As a result, we can capture the tumour’s transition from an avascular to a vascular state. We also account for occlusion of newly formed vessels, assuming that this increases when the ratio of tumour volume to vascular volume is high, this ratio being indicative of the pressure that is being exerted by the tumour cells on the vessels.

From our analysis of the angiogenic and vasculogenic submodels, we conclude that tumours for which angiogenesis or vasculogenesis are dominant can grow in similar ways. In both cases, and for the full model too, the key bifurcation parameter is the ratio of the maximum tumour cell proliferation rate to the apoptosis rate, $1/d_0$. As this parameter varies, the tumour may evolve to an avascular or a vascular steady state or it may undergo exponential growth at a rate which is ultimately determined by the vascular density,

$v/m = 1/\Gamma$, that corresponds to on-switch of TAF production (the discontinuity boundary). Since both submodels have similar bifurcation structures and unbounded growth is exponential in time, we infer that it would be difficult to distinguish between tumours in which angiogenesis or vasculogenesis dominates, on the basis of their growth dynamics alone. By contrast, in Komarova and Mironov (2005), angiogenesis or vasculogenesis always led to unbounded growth with angiogenic tumours growing as a cubic power of time at large times and vasculogenic tumours ultimately growing linearly in time.

Our analysis of the full model shows that both when the tumour evolves to a vascular equilibrium and undergoes exponential growth, the model parameters control the proportion of vasculogenesis-derived vasculature. Our predictions seem consistent with experimental data from different tumours which show a large variation in the proportion of vasculogenesis-derived vasculature (Aghi and Chiocca, 2005). Factors that might determine the proportion of vasculogenic vessels are tumour strain, microenvironment and tumour age (Aghi and Chiocca, 2005). While the predictions in Komarova and Mironov (2005) indicate that, due to depletion of EPCs in the bone marrow and the circulation, angiogenesis will ultimately dominate vasculogenesis, our model suggests that vasculogenesis can be the dominant mechanism at large times. We conclude that in Komarova and Mironov (2005), the effects of vasculogenesis are transient whereas they can persist in our model. The differences in the models' predictions can be explained by the different modelling assumptions made. In Komarova and Mironov (2005), the growth rate of the vasculogenic vessels is simply proportional to the product of the tumour surface area and the level of EPCs in the blood, while the growth rate of angiogenic vessels is only proportional to the tumour surface area (motivated by the fact that vessels mainly grow at the edge of the tumour). Furthermore, the model in Komarova and Mironov (2005) does not include TAF-induced replenishment of EPCs in the bone marrow and does not incorporate EPC and subsequent EC proliferation (once the EPCs have differentiated into ECs) at the tumour site. As a result, in Komarova and Mironov (2005) the levels of EPCs in the bone marrow and the blood decrease at large times, causing angiogenesis to become dominant. Although in the case of unbounded growth, depletion of EPCs in the blood does occur in our model, this does not necessarily mean that the contribution from vasculogenesis decreases. In fact, in our model angiogenesis dominates initially, while vasculogenesis may contribute substantially later. This is consistent with experiments in Spring et al. (2005) which suggest that vasculogenesis becomes more important in the later stages of tumour growth. Further experiments that allow the characterisation of the short- and long-term growth dynamics of angiogenic and vasculogenic tumours would help to compare our predictions and those of Komarova and Mironov (2005).

Analysis of our model shows that vasculogenesis can increase the tumour growth rate. Indeed, from our bifurcation analysis, it follows that when a tumour is growing toward a vascular steady state with new vessels forming via angiogenesis alone, the inclusion of vasculogenesis may push the tumour into unbounded growth. In Stoll et al. (2003), an increase in tumour growth rate was predicted but only observed after a certain time, this being attributed to the time it takes EPCs to mobilise and incorporate into the tumour vasculature. This is consistent with our simulations that show that angiogenesis dominates new vessel formation during early vascular tumour growth. By decreasing k_4 , the rate at which EPCs align into vessels, it is possible to increase further the time required by the EPCs to form functional vasculature (another modelling approach would be to introduce a time delay). A delay in the vasculogenic response was observed in both Tepper et

al. (2005) and Vajkoczy et al. (2003), where the EPCs first arranged themselves in clusters in the interstitial space and, only after 2 weeks and a few days, respectively, formed vascular structures. In our model, it is also possible that an increased growth rate is not observed, even though part of the vasculature is vasculogenesis-derived. This happens if the angiogenic response can meet the demands of the growing tumour, allowing it to grow with maximum vascular density on the discontinuity boundary. In Vajkoczy et al. (2003), a lack of vasculogenic effect was also observed experimentally; even though injected (embryonic) EPCs incorporated into the tumour vasculature, their doing so did not significantly alter the vascular density or the tumour's growth rate.

Our investigation of different treatment strategies reveals that when considering vasculature-targeting therapies, it may, dependent on the parameter values, be necessary to use a combination treatment that inhibits both angiogenesis (ECs) and vasculogenesis (EPCs) to obtain an effective response.

To focus on future work and possible model improvements in the case of unbounded growth, we note that because the proliferation rate of the vessels does not saturate with the TAF concentration, high levels of TAF imply that vessel growth dominates over vessel death. Furthermore, since the tumour growth rate is a saturating function of vascular density, the vessels will grow faster than the tumour at high levels of TAF. Because of this, the vector field in the region where TAF production is active will point toward the discontinuity boundary at large times. At the same time, in the region of no TAF production, the vector field points toward the same boundary, causing unbounded growth to ultimately occur on the discontinuity boundary. By introducing saturating functions for the EC and EPC proliferation terms, as well as the term modelling EPC adherence to the vessel wall, our model could be made more realistic. This would be especially important if the proliferation rates are not very TAF sensitive but saturate quickly as the concentration of TAF is increased. We anticipate that the introduction of saturating functions, in addition to introducing further steady states, could alter the system so that unbounded growth would not necessarily take place on the discontinuity boundary. However, we remark that such a model would still break down at some point in time in the case of unbounded growth, since exponential growth cannot occur indefinitely due to spatial constraints.

Finally, it is also important to bear in mind that tumours are spatially heterogeneous with regions of proliferation, quiescence and necrosis, which cannot always be accurately described by spatially-averaged models; see Breward et al. (2003), Byrne et al. (2006), McDougall et al. (2006) for some examples of models that include spatial effects. Furthermore, because there are many different TAFs and all of these are produced locally, imbalances in pro- and anti-angiogenic substances are also likely to influence the developing vasculature. By explicitly distinguishing between mature and immature vessels, as for instance was done in Arakelyan et al. (2002), our model could be extended to account for different stages of the angiogenic process. It is also possible to amend the model to include tumour interaction with the stroma or normal tissue, which might be important for the progression of tumour growth. In addition, we remark that there has been evidence of a subpopulation of EPCs that release angiogenic factors (Hur et al., 2004) and that our model does not include an effect of that kind. We anticipate that the release of angiogenic factors by EPCs once they have been recruited to the tumour site could further enhance both angiogenesis and vasculogenesis in a paracrine and autocrine fashion.

Acknowledgements

The authors are grateful to the European Commission under the MCRTN and the EPSRC for financial support to IJS and HMB, respectively. The views expressed here are not necessarily those of the European Commission. PKM was partially supported by NIH Grant U56CA113004 from the National Cancer Institute and by a Royal Society-Wolfson Research Merit Award. We also thank the referees for very helpful comments.

Appendix A Nondimensionalisation and model simplification

To nondimensionalise Eqs. (1)–(11), we introduce the following dimensionless variables:

$$\begin{aligned}
 t^* &= \frac{t}{T}, & x^* &= \frac{x}{X}, & y^* &= \frac{y}{Y}, & z^* &= \frac{z}{Z}, \\
 u^* &= \frac{u}{U}, & w^* &= \frac{w}{W}, & v^* &= \frac{v}{V}, \\
 m^* &= \frac{m}{M}, & C_1^* &= \frac{C_1}{C_1}, & C_2^* &= \frac{C_2}{C_2}, & C_3^* &= \frac{C_3}{C_3}, & V_1^* &= \frac{V_1}{V_1},
 \end{aligned}
 \tag{A.1}$$

where the constants T, X, Y and so on are characteristic values of the relevant variable. Using the above rescalings with:

$$\begin{aligned}
 T &= 1/\beta, & X = Y = Z &= \frac{U}{\mu} = \frac{v_0}{\mu}, & U = W = V &= v_0, \\
 M &= \frac{v_0}{\lambda}, & \tilde{C}_1 &= \tilde{C}_2\gamma_1, & \tilde{C}_3 &= \tilde{C}_2\gamma_3 & \text{and} & \tilde{V}_1 &= M,
 \end{aligned}
 \tag{A.2}$$

the model equations transform as follows:

$$\frac{dx^*}{dt^*} = p_1^* + p_2^*C_3^* - k_1^*x^* - k_2^*(C_2^* - \gamma_3C_3^*)x^* - d_1^*x^*,
 \tag{A.3}$$

$$\frac{dy^*}{dt^*} = k_1^*x^* + k_2^*(C_2^* - \gamma_3C_3^*)x^* - k_3^*v^*C_1^*y^* - d_2^*y^*,
 \tag{A.4}$$

$$\frac{dz^*}{dt^*} = k_3^*v^*C_1^*y^* + p_3^*C_1^*z^* - k_4^*z^* - d_3^*z^*,
 \tag{A.5}$$

$$\frac{du^*}{dt^*} = k_4^*z^* + p_5^*C_1^*u^* - \frac{\delta_3^*m^*u^*}{m^* + \delta_4^*v^*} - d_5^*u^*,
 \tag{A.6}$$

$$\frac{dw^*}{dt^*} = p_4^*C_1^*(1 + w^*) - \frac{\delta_1^*m^*w^*}{m^* + \delta_2^*v^*} - d_4^*w^*
 \tag{A.7}$$

$$\frac{dm^*}{dt^*} = \frac{v^*m^*}{v^* + m^*} - d_0^*m^*,
 \tag{A.8}$$

$$\frac{\beta\gamma_1}{q_1\lambda} \left(V_1^* \frac{dC_1^*}{dt^*} + C_1^* \frac{dV_1^*}{dt^*} \right) = c^* m^* H \left(\frac{v_0}{\lambda} (m^* - \Gamma^* v^*) \right) - v^* (C_1^* - C_2^*), \quad (\text{A.9})$$

$$\frac{\beta V_2}{q_1 v_0} \left(\frac{dC_2^*}{dt^*} \right) = \frac{-Q_3}{q_1 v_0} (C_2^* - C_3^*) + v^* (C_1^* - C_2^*) - r^* C_2^*, \quad (\text{A.10})$$

$$\frac{\beta V_3 \gamma_3}{Q_3} \left(\frac{dC_3^*}{dt^*} \right) = (C_2^* - C_3^*), \quad (\text{A.11})$$

$$v^* = w^* + u^* + 1, \quad (\text{A.12})$$

$$V_1^* = m^* + V^* v^*, \quad (\text{A.13})$$

where

$$\begin{aligned} c^* &= \frac{c}{q_1 \lambda \tilde{C}_2}, & d_0^* &= \frac{d_0}{\beta}, & d_1^* &= \frac{d_1}{\beta}, & d_2^* &= \frac{d_2}{\beta}, & d_3^* &= \frac{d_3}{\beta}, \\ d_4^* &= \frac{d_4}{\beta}, & d_5^* &= \frac{d_5}{\beta}, & \delta_1^* &= \frac{\delta_1}{\beta}, & \delta_2^* &= \delta_2 \lambda, & \delta_3^* &= \frac{\delta_3}{\beta}, & \delta_4^* &= \delta_4 \lambda, \\ \Gamma^* &= \Gamma \lambda, & k_1^* &= \frac{k_1}{\beta}, & k_2^* &= \frac{k_2 \tilde{C}_2}{\beta}, & k_3^* &= \frac{k_3 v_0 \tilde{C}_2 \gamma_1}{\beta}, \\ k_4^* &= \frac{k_4}{\beta}, & p_1^* &= \frac{p_1 \mu}{\beta v_0}, & p_2^* &= \frac{p_2 \tilde{C}_2 \gamma_3 \mu}{\beta v_0}, & p_3^* &= \frac{p_3 \tilde{C}_2 \gamma_1}{\beta}, \\ p_4^* &= \frac{p_4 \tilde{C}_2 \gamma_1}{\beta}, & p_5^* &= \frac{p_5 \tilde{C}_2 \gamma_1}{\beta}, & r^* &= \frac{r V_2}{q_1 v_0} \quad \text{and} \quad V^* = \lambda \end{aligned} \quad (\text{A.14})$$

are dimensionless parameters. We assume that the timescales inherent in the TAF mass balance equations are short in comparison to the timescale given by the tumour growth rate, $T = 1/\beta$, i.e.

$$\mathcal{O}(\beta) \ll \mathcal{O}\left(\frac{c}{\tilde{C}_2 \gamma_1}\right) = \mathcal{O}\left(\frac{q_1 \lambda}{\gamma_1}\right) = \mathcal{O}\left(\frac{q_1 v_0}{V_2}\right) = \mathcal{O}\left(\frac{Q_3}{V_2}\right) = \mathcal{O}(r) = \mathcal{O}\left(\frac{Q_3}{V_3 \gamma_3}\right). \quad (\text{A.15})$$

Under this assumption (A.9)–(A.11) are quasi-steady at leading order and by solving explicitly for C_1^* , C_2^* and C_3^* :

$$C_1^* = \frac{(v^* + r^*) c^* m^* H(m^* - \Gamma^* v^*)}{v^* r^*}, \quad (\text{A.16})$$

$$C_3^* = C_2^* = \frac{v^* C_1^*}{v^* + r^*} = \frac{c^* m^* H(m^* - \Gamma^* v^*)}{r^*}. \quad (\text{A.17})$$

Substitution of (A.16) and (A.17) into (A.3)–(A.8) yields our model equations:

$$\begin{aligned} \frac{dx^*}{dt^*} &= p_1^* + \hat{p}_2 m^* H(m^* - \Gamma^* v^*) - k_1^* x^* \\ &\quad - \hat{k}_2 m^* x^* H(m^* - \Gamma^* v^*) - d_1^* x^*, \end{aligned} \quad (\text{A.18})$$

$$\begin{aligned} \frac{dy^*}{dt^*} &= k_1^* x^* + \hat{k}_2 m^* x^* H(m^* - \Gamma^* v^*) \\ &\quad - \hat{k}_3 (v^* + r^*) m^* y^* H(m^* - \Gamma^* v^*) - d_2^* y^*, \end{aligned} \quad (\text{A.19})$$

$$\begin{aligned} \frac{dz^*}{dt^*} &= \hat{k}_3 (v^* + r^*) m^* y^* H(m^* - \Gamma^* v^*) \\ &\quad + \frac{\hat{p}_3 (v^* + r^*) m^* z^* H(m^* - \Gamma^* v^*)}{v^*} - k_4^* z^* - d_3^* z^*, \end{aligned} \quad (\text{A.20})$$

$$\frac{du^*}{dt^*} = k_4^* z^* + \frac{\hat{p}_5 (v^* + r^*) m^* u^* H(m^* - \Gamma^* v^*)}{v^*} - \frac{\delta_3^* m^* u^*}{m^* + \delta_4^* v^*} - d_5^* u^*, \quad (\text{A.21})$$

$$\frac{dw^*}{dt^*} = \frac{\hat{p}_4 (v^* + r^*) m^* (1 + w^*) H(m^* - \Gamma^* v^*)}{v^*} - \frac{\delta_1^* m^* w^*}{m^* + \delta_2^* v^*} - d_4^* w^*, \quad (\text{A.22})$$

$$\frac{dm^*}{dt^*} = \left(\frac{v^*}{v^* + m^*} - d_0^* \right) m^*, \quad (\text{A.23})$$

$$v^* = w^* + u^* + 1, \quad (\text{A.24})$$

where

$$\begin{aligned} \hat{k}_2 &= \frac{k_2^* (1 - \gamma_3) c^*}{r^*}, & \hat{k}_3 &= \frac{k_3^* c^*}{r^*}, & \hat{p}_2 &= \frac{p_2^* c^*}{r^*}, & \hat{p}_3 &= \frac{p_3^* c^*}{r^*}, \\ \hat{p}_4 &= \frac{p_4^* c^*}{r^*} & \text{and} & & \hat{p}_5 &= \frac{p_5^* c^*}{r^*} \end{aligned} \quad (\text{A.25})$$

are dimensionless parameter groupings.

Appendix B Model variables and parameters

The model variables and parameters are presented in Tables B.1 and B.2, respectively.

B.1 Parameter values

Below we discuss the values of the model parameters and give estimates for some of them. However, it is important to note that the parameter values are likely to vary considerably between different tumours. Hence, we use these values for illustrative purposes.

The main bifurcation parameter is the dimensionless ratio $1/d_0^* = \beta/d_0$. The maximum tumour growth rate, β , is related to a corresponding potential doubling time, T_{pot} (T_{pot} is defined as the time it would take for a tumour to double in size if there were no cell loss), by the relation $T_{\text{pot}} = \ln 2/\beta$. Assuming that β gives rise to a potential doubling time of one day (22 h in Tannock, 1970), we have that $\beta \approx 0.69/\text{day}$. The rate of apoptosis then determines the actual doubling time associated with β . For example, if $d_0 = 0.15\beta$ then the doubling time is $\ln 2/(\beta - d_0) = 1/0.85 \approx 1.18$ days and our bifurcation parameter $1/d_0^* \approx 6.7$, while if $d_0 = 0.8\beta$ then the doubling time is 5 days and the bifurcation parameter $1/d_0^* = 1.25$.

Table B.1 Model variables

Variable	Dimension	Description
C_1	ML^{-3}	Concentration of TAF in the tumour
C_2	ML^{-3}	Concentration of TAF in the blood
C_3	ML^{-3}	Concentration of TAF in the bone marrow
m	L^3	Tumour volume (cells and interstitium)
t	T	Time
u	L^3	Vasculogenesis-derived tumour vasculature
v	L^3	Total volume of tumour vasculature
V_1	L^3	Total tumour tissue volume (cells, interstitium vasculature)
w	L^3	Angiogenesis-derived tumour vasculature
x	1	Number of EPCs in the bone marrow
y	1	Number of EPCs in the blood
z	1	Number of EPCs in the tumour

Once $1/d_0^* = \beta/d_0$ is fixed, $\Gamma^* = \Gamma\lambda$ determines the outcome of the system (recall Fig. 3 where there is a stable avascular steady state if $1 < 1/d_0 < \Gamma + 1$, while the tumour either evolves to a vascular steady state or grows exponentially if $1/d_0 \geq \Gamma + 1$). We have been unable to establish a value of Γ and λ . In our simulations we take $\Gamma^* = 4$, assuming that $\lambda = 0.1$ and that neovascularisation is initiated at a vascular density of 0.025 (i.e. a vascular space of 2.5%) equivalent to $\Gamma = 40$. We note that the vascular space of tumour tissue varies considerably, as reviewed in Jain (1988), from 0.4% to 27.5%.

By taking the volume of an avascular tumour to correspond to a radius of 1 mm (assuming that avascular tumours do not grow larger than a diameter of 1–2 mm), and by assuming that neovascularisation is initiated at a vascular density of $1/\Gamma = 0.025$, we approximate the background vasculature, v_0 , to be $0.025 \times 4\pi \times 1^3/3 \text{ mm}^3 \approx 0.1 \text{ mm}^3$.

The potential doubling time of ECs in activated endothelium, e.g. due to mechanical injury or tumour growth, is roughly 50 h (Tannock, 1970; Tannock and Hayashi, 1972). This value is in accordance with Mantzaris et al. (2004) where the EC doubling time during angiogenesis was said to be “a few days”. If we assume that a potential doubling time of 2 days corresponds to a TAF (VEGF) level of 10 ng/ml, and also choose this as the characteristic level in the tumour, $\tilde{C}_1 = \tilde{C}_2\gamma_1 = 10 \text{ ng/ml}$, we have that $p_4^* = \frac{p_4\tilde{C}_2\gamma_1}{\beta} = 0.5$. A VEGF level of 10 ng/ml for most rapid EC proliferation is consistent with experiments which measured DNA synthesis of HUVECs proliferating in response to VEGF (Soker et al., 1997). Furthermore, a VEGF level of 10 ng/ml is comparable with levels measured in some tumours (Kraft et al., 1999).

In Song et al. (2005), the percentage of endothelial cells that were apoptotic in the tumour tissue was determined to 1.5%. If we assume that the duration of apoptosis is 3 hours (Thompson et al., 1992), then the rate of cell loss can be estimated to $0.015/(3/24)/\text{day} = 0.12/\text{day}$. This gives $d_4^* = d_4/\beta \approx 0.17$.

The parameter c corresponding to production of TAF per unit tumour volume per day is given in Stoll et al. (2003) to be $7.0 \times 10^2 \text{ pg/mm}^3/\text{day}$.

The decay rate of TAF in the blood, r , can be obtained from the half-life of VEGF in blood, $T_{1/2}$, which, from Stoll et al. (2003), is approximately 3 min. This gives $r \approx \ln 2/T_{1/2} = 330/\text{day}$.

Table B.2 Model parameters

Parameter	Dimension	Parameter description
β	T^{-1}	Maximum tumour growth rate
c	$MT^{-1}L^{-3}$	Production rate of TAF per unit tumour volume
d_0	T^{-1}	Per capita death rate of tumour volume
d_1	T^{-1}	Per capita death rate of EPCs in the bone marrow
d_2	T^{-1}	Per capita death/uptake rate of EPCs in the blood
d_3	T^{-1}	Per capita death rate of EPCs in the tumour
d_4	T^{-1}	Per capita death rate of angiogenic vasculature
d_5	T^{-1}	Per capita death rate of vasculogenic vasculature
δ_1	T^{-1}	Maximum rate of angiogenic vessel occlusion
δ_2	1	Value of m/v where angiogenic occlusion attains half-maximal value
δ_3	T^{-1}	Maximum rate of vasculogenic vessel occlusion
δ_4	1	Value of m/v where vasculogenic occlusion attains half-maximal value
γ_1	1	Tumour/blood partition coefficient
γ_3	1	Bone marrow/blood partition coefficient
Γ	1	Value of m/v above which TAF production is active
k_1	T^{-1}	Per capita delivery rate of EPCs from the bone marrow to blood
k_2	$L^3M^{-1}T^{-1}$	Per capita delivery rate of EPCs from the bone marrow to blood per unit TAF
k_3	$T^{-1}M^{-1}$	Per capita adherence rate of EPCs per unit TAF and unit tumour vasculature
k_4	T^{-1}	Per capita alignment rate of EPCs into functional tumour vasculature
λ	1	Value of v/m where tumour growth rate attains half-maximal value
μ	L^3	Functional vasculature volume per EPC
p_1	T^{-1}	Constant production rate of EPC in the bone marrow
p_2	$L^3M^{-1}T^{-1}$	Production rate of EPC in the bone marrow per unit TAF concentration
p_3	$L^3M^{-1}T^{-1}$	Per capita production rate of EPC at tumour site per unit TAF concentration
p_4	$L^3M^{-1}T^{-1}$	Per capita production rate of angiogenic vessels per unit TAF
p_5	$L^3M^{-1}T^{-1}$	Per capita production rate of vasculogenic vessels per unit TAF
q_1	T^{-1}	Blood flow rate to the tumour per unit vasculature
Q_3	L^3T^{-1}	Blood flow to the bone marrow
r	T^{-1}	Decay rate of TAF in the blood
v_0	L^3	Initial background vasculature volume
V_2	L^3	Volume of blood
V_3	L^3	Volume of bone marrow

The characteristic value of the concentration of TAF in the blood, \tilde{C}_2 , is, as given in Stoll et al. (2003), $1 \text{ ng/ml} = 10^{-12} \text{ g/mm}^3$.

We take the volume of blood, V_2 , to be equal to the value of plasma volume, which in Gerlowski and Jain (1983) is given to be $1.0 \times 10^3 \text{ mm}^3$.

In Oku et al. (1998), the blood flow for wild type human melanoma intracerebral xenografts was given as 105 ml/min/100 g with a corresponding blood volume in the tumour of 1.99 ml/100 g. From these values, we estimate $q_1 = 105 \text{ ml} \times 24 \times 60/1.99/\text{day} \approx 76000/\text{day}$.

With the above estimates, we obtain that $c^* \approx 0.09$, $r^* \approx 43$ and $\hat{p}_4 \approx 0.001$.

In Stoll et al. (2003), the number of ECs per unit vascular volume was estimated to be $4.9 \times 10^5/\text{mm}^3$. If we assume that the same holds true for EPCs, then we have that μ , the vasculature volume per EPC, is $1/(4.9 \times 10^5) \approx 0.2 \times 10^{-5} \text{ mm}^3$. With $v_0 = 0.1$ we obtain the scaling factors $X = Y = Z = U/\mu = v_0/\mu = 0.1/0.2/10^{-5} = 50,000$.

In Hristov et al. (2003), the number of EPCs in blood of healthy individuals is stated to be approximately between 70 to 210 cells/ml, while in Dome et al. (2006) the number of EPCs in healthy individuals was estimated to 345 cells/ml. Assuming background levels of 300 cells/ml in mice, with a blood volume as above (1.0 ml), we obtain that the (dimensionless) background level of EPCs in the blood as given by (38) should correspond to $y/Y = 300/50000 = 0.006$. Thus, we choose k_1^* , p_1^* , d_2^* and d_1^* to obtain this level. We do not know the background level of EPCs in the bone marrow, but assuming that it is higher than in blood, since under normal conditions EPCs reside predominantly in the bone marrow (Hattori et al., 2001), we choose $k_1^* < d_2^*$ as this guarantees $x > y$.

Based on the above estimates (where possible), unless otherwise stated, in the full model we used the following dimensionless parameter values:

$$\begin{aligned} d_1^* &= 0.1, & d_2^* &= 0.4, & d_3^* &= 0.25, & d_4^* &= 0.17, & d_5^* &= 0.17, \\ \delta_1^* &= 0.15, & \delta_2^* &= 0.6, & \delta_3^* &= 0.15, & \delta_4^* &= 0.6, & \Gamma^* &= 4, \\ k_1^* &= 0.03, & \hat{k}_2 &= 0.002, & \hat{k}_3 &= 0.0002, & k_4^* &= 0.5, & & \\ p_1^* &= 0.01, & \hat{p}_2 &= 0.002, & \hat{p}_3 &= 0.002, & \hat{p}_4 &= 0.001, & & \\ \hat{p}_5 &= 0.001 & \text{and} & r^* &= 43. \end{aligned} \tag{B.1}$$

To generate the schematic bifurcation diagram and phase plane for the angiogenesis submodel, Figs. 3 and 4, we used the following dimensionless parameter values:

$$d_4^* = 3, \quad \delta_1^* = 5, \quad \delta_2^* = 1, \quad \Gamma^* = 4, \quad \hat{p}_4 = 0.07 \quad \text{and} \quad r^* = 4. \tag{B.2}$$

Note that in the angiogenesis submodel $\hat{p}_2 = \hat{k}_2 = \hat{k}_3 = 0$ while in the vasculogenesis submodel $\hat{p}_4 = 0$.

Appendix C Analysis of Eq. (42)

The number of physically realistic roots of (42) can be determined as follows. From (46), we notice that all zeros of $f(u)$ are negative, $f(u) > 0$ if $u \geq 0$ (assuming $1/d_0 - 1 > 0$ for vascular steady states) and that $f(u) \rightarrow \infty$ as $u \rightarrow \infty$. From (43), it follows that

$$\left. \frac{dg}{du} \right|_{u=0} = p_4 p_3 k_3 k_2 \left(\frac{1}{d_0} - 1 \right)^4 \prod_{i=1}^5 (-G_i). \tag{C.1}$$

Since $G_3G_4 > 0$ and $G_5 < 0$, we deduce that $\frac{dg}{du}|_{u=0} < 0$, if and only if G_1 and G_2 are of opposite signs. Therefore, if $\frac{dg}{du}|_{u=0} < 0$, then there exists only one positive zero of $g(u)$ (G_1 or G_2). In addition, since $g(0) = 0$, $f(u) > 0$ for all $u \geq 0$ and the fact that $g(u) \rightarrow \infty$ as $u \rightarrow \infty$ and does so faster than the fourth-order function $f(u)$ implies that when $\frac{dg}{du}|_{u=0} < 0$, there will always exist one and only one positive root, say \hat{u} , of (42). However, further analysis reveals that this root corresponds to an unrealistic steady state. This is because $\hat{u} > \max\{G_1, G_2\}$ and if $u > G_2$ then $z < 0$ always holds. Similarly, in the case $\frac{dg}{du}|_{u=0} = 0$, we also conclude that only physically unrealistic steady states can exist (again $z < 0$ at the steady states). A necessary condition for physically realistic steady states is therefore $\frac{dg}{du}|_{u=0} > 0$. As above, we conclude that if $\frac{dg}{du}|_{u=0} > 0$ and both G_1 and G_2 are negative, only physically unrealistic equilibrium points can exist. Therefore, only if G_1 and G_2 both are positive, so that $g(u)$ has two positive zeros, might there be one or two physically realistic steady states in addition to the physically unrealistic steady state where $z < 0$. (This will occur whenever the parameters are such that $\bar{f} \geq 0$ at $\min\{u^* > 0 : \bar{f}'|_{u=u^*} = 0\}$). Hence the sixth-order polynomial has at most two physically realistic solutions.

References

- Aghi, M., Chiocia, E.A., 2005. Contribution of bone marrow-derived cells to blood vessels in ischemic tissues and tumors. *Mol. Ther.* 12(6), 994–1005.
- Amidon, G.L., Lee, P.I., Topp, E.M., 2000. *Transport Processes in Pharmaceutical Systems*. Dekker, New York.
- Arakelyan, L., Vainstein, V., Agur, Z., 2002. A computer algorithm describing the process of vessel formation and maturation, and its use for predicting the effects of anti-angiogenic and anti-maturation therapy on vascular tumor growth. *Angiogenesis* 5(3), 203–214.
- Asahara, T., Murohara, T., Sullivan, A., Silver, M., van der Zee, R., Li, T., Witzenbichler, B., Schatteman, G., Isner, J.M., 1997. Isolation of putative endothelial cells for angiogenesis. *Science* 275(5302), 964–967.
- Asahara, T., Takahashi, T., Masuda, H., Kalka, C., Chen, D., Iwaguro, H., Inai, Y., Silver, M., Isner, J.M., 1999. VEGF contributes to postnatal neovascularization by mobilizing bone marrow-derived endothelial progenitor cells. *EMBO J.* 18(14), 3964–3972.
- Bolontrade, M.F., Zhou, R.-R., Kleinerman, E.S., 2002. Vasculogenesis plays a role in the growth of Ewing's sarcoma *in Vivo*. *Clin. Cancer Res.* 8(11), 3622–3627.
- Breward, C.J.W., Byrne, H.M., Lewis, C.E., 2003. A multiphase model describing vascular tumour growth. *Bull. Math. Biol.* 65(4), 609–640.
- Byrne, H.M., Owen, M.R., Alarcón, T., Murphy, J., Maini, P.K., 2006. Modelling the response of vascular tumours to chemotherapy: a multiscale approach. *Math. Models Methods Appl. Sci.* 16(Suppl. Issue 1), 1219–1241.
- Carmeliet, P., 2003. Angiogenesis in health and disease. *Nat. Med.* 9(6), 653–660.
- Carmeliet, P., Jain, R.K., 2000. Angiogenesis in cancer and other diseases. *Nature* 407(6801), 249–257.
- di Bernardo, M., Budd, C., Champneys, A.R., Kowalczyk, P., Nordmark, A.B., Olivar, G., Piironen, P.T., Bifurcations in nonsmooth dynamical systems. BCANM Preprint 2005.4, <http://www.enm.bris.ac.uk/ann/preprints/2005r04.html>.
- Dome, B., Timar, J., Dobos, J., Meszaros, L., Raso, E., Paku, S., Kenessey, I., Ostoros, G., Magyar, M., Ladanyi, A., Bogos, K., Továri, J., 2006. Identification and clinical significance of circulating endothelial progenitor cells in human non-small cell lung cancer. *Cancer Res.* 66(14), 7341–7347.
- Drake, C.J., 2003. Embryonic and adult vasculogenesis. *Birth Defects Res. Part C* 69(1), 73–82.
- Duda, D.G., Cohen, K.S., Kozin, S.V., Perentes, J.Y., Fukumura, D., Scadden, D.T., Jain, R.K., 2006. Evidence for incorporation of bone marrow-derived endothelial cells into perfused blood vessels in tumors. *Blood* 107(7), 2774–2776.
- Ermentrout, B., 2002. *Simulating, Analyzing, and Animating Dynamical Systems. A Guide to XPPAUT for Researchers and Students*. SIAM, Philadelphia.

- Folkman, J., 1971. Tumor angiogenesis: therapeutic implications. *N. Engl. J. Med.* 285(21), 1182–1186.
- Gerlowski, L.E., Jain, R.K., 1983. Physiologically based pharmacokinetic modeling: principles and applications. *J. Pharm. Sci.* 72(10), 1103–1127.
- Gill, M., Dias, S., Hattori, K., Rivera, M.L., Hicklin, D., Witte, L., Girardi, L., Yurt, R., Himel, H., Rafii, S., 2001. Vascular trauma induces rapid but transient mobilization of VEGFR2+AC133+ endothelial precursor cells. *Circ. Res.* 88(2), 167–174.
- Griffon-Etienne, G., Boucher, Y., Brekken, C., Suit, H.D., Jain, R.K., 1999. Taxane-induced apoptosis decompresses blood vessels and lowers interstitial fluid pressure in solid tumours: clinical implications. *Cancer Res.* 59(15), 3776–3782.
- Harris, A.L., 2002. Hypoxia—a key regulatory factor in tumour growth. *Nat. Rev. Cancer* 2(1), 38–47.
- Hattori, K., Dias, S., Heissig, B., Hackett, N.R., Lyden, D., Tateno, M., Hicklin, D.J., Zhu, Z., Witte, L., Crystal, L.G., Moore, M.A.S., Rafii, S., 2001. Vascular endothelial growth factor and angiopoietin-1 stimulate postnatal hematopoiesis by recruitment of vasculogenic and hematopoietic stem cells. *J. Exp. Med.* 193(9), 1005–1014.
- Heissig, B., Hattori, K., Dias, S., Friedrich, M., Ferris, B., Hackett, N.R., Crystal, R.G., Besmer, P., Lyden, D., Moore, M.A.S., Werb, Z., Rafii, S., 2002. Recruitment of stem and progenitor cells from the bone marrow niche requires MMP-9 mediated release of Kit-ligand. *Cell* 109(5), 625–637.
- Helmlinger, G., Netti, P.A., Lichtenbeld, H.C., Melder, R.J., Jain, R.K., 1997. Solid stress inhibits the growth of multicellular tumor spheroids. *Nat. Biotech.* 15(8), 778–783.
- Hoeben, A., Landuyt, B., Highley, M.S., Wildiers, H., Van Oosterom, A.T., De Bruijn, E.A., 2004. Vascular endothelial growth factor and angiogenesis. *Pharmacol. Rev.* 56(4), 549–580.
- Hristov, M., Erl, W., Weber, P.C., 2003. Endothelial progenitor cells, mobilization, differentiation and homing. *Art. Thromb. Vasc. Biol.* 23(7), 1185–1189.
- Hunting, C.B., Noort, W.A., Zwaginga, J.J., 2005. Circulating endothelial (progenitor) cells reflect the state of the endothelium: vascular injury, repair and neovascularization. *Vox Sang.* 88(1), 1–9.
- Hur, J., Yoon, C.-H., Kim, H.-S., Choi, J.-H., Kang, H.-J., Hwang, K.-K., Oh, B.-H., Lee, M.-M., Park, Y.-B., 2004. Characterization of two types of endothelial progenitor cells and their different contributions to neovascularogenesis. *Art. Thromb. Vasc. Biol.* 24(2), 288–293.
- Jain, R.K., 1988. Determinants of tumor blood flow: a review. *Cancer Res.* 48, 2641–2658.
- Jain, R.K., 2003. Molecular regulation of vessel maturation. *Nat. Med.* 9(6), 685–693.
- Jin, H., Aiyer, A., Su, J., Borgstrom, P., Stupack, D., Friedlander, M., Varner, J., 2006. A homing mechanism for bone marrow-derived progenitor cell recruitment to the neovasculature. *J. Clin. Invest.* 116(3), 652–662.
- Jordan, D.W., Smith, P., 1999. *Nonlinear Ordinary Differential Equations. An Introduction to Dynamical Systems*, 3rd edn. Oxford University Press, Oxford.
- Ke, L.D., Shi, Y.-X., Im, S.-A., Chen, X., Yung, W.K.A., 2000. The relevance of cell proliferation, vascular endothelial growth factor production, and basic fibroblast growth factor production to angiogenesis and tumorigenicity in human glioma cell lines. *Clin. Cancer Res.* 6, 2562–2572.
- Khakoo, A.Y., Finkel, T., 2005. Endothelial progenitor cells. *Annu. Rev. Med.* 56, 79–101.
- Kim, H.K., Song, K.S., Kim, H.O., Chung, J.-H., Lee, K.R., Lee, Y.-J., Lee, D.H., Lee, E.S., Kim, H.K., Ryu, K.W., Bae, J.-M., 2003. Circulating numbers of endothelial progenitor cells in patients with gastric and breast cancer. *Cancer Lett.* 198(1), 83–88.
- Kolomecki, K., Stepien, H., Bartos, M., Kuzdak, K., 2001. Usefulness of VEGF, MMP-2, MMP-3 and TIMP-2 serum level evaluation in patients with adrenal tumours. *Endo. Reg.* 35(1), 9–16.
- Komarova, N.L., Mironov, V., 2005. On the role of endothelial progenitor cells in tumor neovascularization. *J. Theor. Biol.* 235(3), 338–349.
- Kraft, A., Weindel, K., Ochs, A., Marth, C., Zmija, J., Schumacher, P., Unger, C., Marme, D., Gastl, G., 1999. Vascular endothelial growth factor in the sera and effusions of patients with malignant and nonmalignant disease. *Cancer* 85, 178–187.
- Leine, R.I., van Campen, D.H., van de Vrande, B.L., 2000. Bifurcations in nonlinear discontinuous systems. *Nonlin. Dyn.* 23(2), 105–164.
- Li, H., Gerald, W.L., Benezra, R., 2004. Utilization of bone marrow-derived endothelial cell precursors in spontaneous prostate tumors varies with tumor grade. *Cancer Res.* 64(17), 6137–6143.
- Li, B., Sharpe, E.E., Maupin, A.B., Teleron, A.A., Pyle, A.L., Carmeliet, P., Young, P.P., 2006. VEGF and PlGF promote adult vasculogenesis by enhancing EPC recruitment and vessel formation at the site of tumor neovascularization. *FASEB J.* 20, E664–E676.
- Lyden, D., Hattori, K., Dias, S., Costa, C., Blaikie, P., Butros, L., Chadburn, A., Heissig, B., Marks, W., Witte, L., Wu, Y., Hicklin, D., Zhu, Z., Hackett, N.R., Crystal, R.G., Moore, M.A.S., Hajar, K.A.,

- Manova, K., Benezra, R., Rafii, S., 2001. Impaired recruitment of bone-marrow-derived endothelial and hematopoietic precursor cells blocks tumour angiogenesis and growth. *Nat. Med.* 7(11), 1194–1201.
- Mantzaris, N.V., Webb, S., Othmer, H.G., 2004. Mathematical modeling of tumor-induced angiogenesis. *J. Math. Biol.* 49(2), 111–187.
- McDougall, S.R., Anderson, A.R.A., Chaplain, M.A.J., 2006. Mathematical modelling of dynamic adaptive tumour-induced angiogenesis: clinical implications and therapeutic targeting strategies. *J. Theor. Biol.* 241(3), 564–589.
- Moore, M.A.S., Hattori, K., Heissig, B., Shieh, J.-H., Dias, S., Crystal, R.G., Rafii, S., 2001. Mobilization of endothelial and hematopoietic stem and progenitor cells by adenovector-mediated elevation of serum levels of SDF-1, VEGF, and angiopoietin-1. *Ann. New York Acad. Sci.* 938, 36–47.
- Murray, J.D., 1993. *Mathematical Biology*, 2nd edn. Springer, New York.
- Oku, T., Tjuvajev, J.G., Miyagawa, T., Sasajima, T., Joshi, A., Joshi, R., Finn, R., Claffey, K.P., Blasberg, R.G., 1998. Tumor growth modulation by sense and antisense vascular endothelial growth factor gene expression: effects on angiogenesis, vascular permeability, blood volume, blood flow, fluorodeoxyglucose uptake, and proliferation of human melanoma intracerebral xenografts. *Cancer Res.* 58(18), 4185–4192.
- Padera, T.P., Stoll, B.R., Tooredman, J.B., Capen, D., di Tomaso, E., Jain, R.K., 2004. Cancer cells compress intratumour vessels. *Nature* 427(6976), 695.
- Peters, B.A., Diaz, L.A. Jr., Polyak, K., Meszler, L., Romans, K., Guinan, E.C., Antin, J.H., Myerson, D., Hamilton, S.R., Vogelstein, B., Kinzler, K.W., Lengauer, C., 2005. Contribution of bone marrow-derived endothelial cells to human tumor vasculature. *Nat. Med.* 11(3), 261–262.
- Rafii, S., Lyden, D., Benezra, R., Hattori, K., Heissig, B., 2002. Vascular and haematopoietic stem cells: novel targets for anti-angiogenesis therapy?. *Nat. Rev. Cancer* 2(11), 826–835.
- Ribatti, D., 2004. The involvement of endothelial progenitor cells in tumor angiogenesis. *J. Cell Mol. Med.* 8(3), 294–300.
- Risau, W., Flamme, I., 1995. Vasculogenesis. *Annu. Rev. Cell Dev. Biol.* 11, 73–91.
- Schatteman, G.C., Awad, O., 2004. Hemangioblasts, angioblasts, and adult endothelial cell progenitors. *Anat. Rec. Part A* 276, 13–21.
- Shargel, L., Yu, A.B.C., 1999. *Applied Biopharmaceutics & Pharmacokinetics*, 4th edn. Appleton & Lange.
- Soker, S., Gollamudi-Payne, S., Fidler, H., Charmahelli, H., Klagsbrun, M., 1997. Inhibition of vascular endothelial growth factor (VEGF)-induced endothelial cell proliferation by a peptide corresponding to the exon 7-encoded domain of VEGF₁₆₅. *J. Biol. Chem.* 272(50), 31582–31588.
- Song, S., Ewald, A.J., Stallcup, W., Werb, Z., Bergers, G., 2005. PDGFR β ⁺ perivascular progenitor cells in tumours regulate pericyte differentiation and vascular survival. *Nat. Cell Biol.* 7(9), 870–879.
- Spring, H., Schüler, T., Arnold, B., Hämmerling, G.J., Ganss, R., 2005. Chemokines direct endothelial progenitors into tumor neovessels. *Proc. Natl. Acad. Sci. USA* 102(50), 18111–18116.
- Stoll, B.R., Migliorini, C., Kadambi, A., Munn, L.L., Jain, R.K., 2003. A mathematical model of the contribution of endothelial progenitor cells to angiogenesis in tumor: implications for antiangiogenic therapy. *Blood* 102(7), 2555–2561.
- Sussman, L.K., Upalakalin, J.N., Roberts, M.J., Kocher, O., Benjamin, L.E., 2003. Blood markers for vasculogenesis increase with tumour progression in patients with breast carcinoma. *Cancer Biol. Ther.* 2(3), 255–256.
- Tannock, I.F., 1970. Population kinetics of carcinoma cells, capillary endothelial cells, and fibroblasts in a transplanted mouse mammary tumor. *Cancer Res.* 30, 2470–2476.
- Tannock, I.F., Hayashi, S., 1972. The proliferation of capillary endothelial cells. *Cancer Res.* 32, 77–82.
- Tepper, O.M., Capla, J.M., Galiano, R.D., Ceradini, D.J., Callaghan, M.J., Kleinman, M.E., Gurtner, G.C., 2005. Adult vasculogenesis occurs through in situ recruitment, proliferation, and tubulization of circulating bone marrow-derived cells. *Blood* 105(3), 1068–1077.
- Thompson, H.J., Strange, R., Schedin, P.J., 1992. Apoptosis in the genesis and prevention of cancer. *Cancer Epidemiol. Biomark. Prev.* 1, 597–602.
- Vajkoczy, P., Blum, S., Lamparter, M., Mailhammer, R., Erber, R., Engelhardt, B., Vestweber, D., Hatzipoulos, A.K., 2003. Multistep nature of microvascular recruitment of ex vivo-expanded embryonic endothelial progenitor cells during tumor angiogenesis. *J. Exp. Med.* 197(12), 1755–1765.